Turun yliopisto
University of Turku

FLUVIO-MORPHOLOGICAL PROCESSES OF MEANDER BENDS – COMBINING CONVENTIONAL FIELD MEASUREMENTS, CLOSE-RANGE REMOTE SENSING AND COMPUTATIONAL MODELLING

Elina Kasvi

TURUN YLIOPISTON JULKAISUJA – ANNALES UNIVERSITATIS TURKUENSIS
Sarja - ser. A II osa - tom. 298 | Biologica - Geographica - Geologica | Turku 2015

University of Turku

Faculty of Mathematics and Natural Sciences
Department of Geography and Geology
Geography Division

Supervised by

Adjunct Professor Petteri Alho
Department of Geography and geology
University of Turku

Professor Hannu Hyyppä
Department of Real Estate, Planning and Geoinformatics
Aalto University

Reviewed by

Professor Stephen Darby
Department of Geography and Environment
University of Southampton

Professor Stuart N. Lane
Faculty of Geosciences and Environment
University of Lausanne

Opponent

Professor Janet Hooke
Department of Geography and Planning
University of Liverpool

The originality of this thesis has been checked in accordance with the University of Turku quality assurance system using the Turnitin OriginalityCheck service.

ISBN 978-951-29-6004-0 (PRINT)
ISBN 978-951-29-6005-7 (PDF)
ISSN 0082-6979
Painosalama Oy - Turku, Finland 2015

ABSTRACT

Meandering rivers have been perceived to evolve rather similarly around the world independently of the location or size of the river. Despite the many consistent processes and characteristics they have also been noted to show complex and unique sets of fluvio-morphological processes in which local factors play important role. These complex interactions of flow and morphology affect notably the development of the river. Comprehensive and fundamental field, flume and theoretically based studies of fluvio-morphological processes in meandering rivers have been carried out especially during the latter part of the 20th century. However, as these studies have been carried out with traditional field measurements techniques their spatial and temporal resolution is not competitive to the level achievable today. The hypothesis of this study is that, by exploiting the increased spatial and temporal resolution of the data, achieved by combining conventional field measurements with a range of modern technologies, will provide new insights to the spatial patterns of the flow-sediment interaction in meandering streams, which have perceived to show notable variation in space and time. This thesis shows how the modern technologies can be combined to derive very high spatial and temporal resolution data on fluvio-morphological processes over meander bends. The flow structure over the bends is recorded in situ using acoustic Doppler current profiler (ADCP) and the spatial and temporal resolution of the flow data is enhanced using 2D and 3D CFD over various meander bends. The CFD are also exploited to simulate sediment transport. Multi-temporal terrestrial laser scanning (TLS), mobile laser scanning (MLS) and echo sounding data are used to measure the flow-based changes and formations over meander bends and to build the computational models. The spatial patterns of erosion and deposition over meander bends are analysed relative to the measured and modelled flow field and sediment transport. The results are compared with the classic theories of the processes in meander bends. Mainly, the results of this study follow well the existing theories and results of previous studies. However, some new insights regarding to the spatial and temporal patterns of the flow-sediment interaction in a natural sand-bed meander bend are provided. The results of this study show the advantages of the rapid and detailed measurements techniques and the achieved spatial and temporal resolution provided by CFD, unachievable with field measurements. The thesis also discusses the limitations which remain in the measurement and modelling methods and in understanding of fluvial geomorphology of meander bends. Further, the hydro- and morphodynamic models' sensitivity to user-defined parameters is tested, and the modelling results are assessed against detailed field measurement. The study is implemented in the meandering sub-Arctic Pulmanki River in Finland. The river is unregulated and sand-bed and major morphological changes occur annually on the meander point bars, which are inundated only during the snow-melt-induced spring floods. The outcome of this study applies to sand-bed meandering rivers in regions where normally one significant flood event occurs annually, such as Arctic areas with snow-melt induced spring floods, and where the point bars of the meander bends are inundated only during the flood events.

ACKNOWLEDGEMENTS

After making my rather hard decision to become a Ph.D. student I have not regretted it for a moment. This work has offered me many opportunities and experiences which I would never have gotten otherwise. It has taken me to various places around the world from Arctic to the Pacific Ocean. During those field and conference trips I have learned a lot and met many interesting people. Those trips have been very motivating and eye opening. Even though I have also spent vast amount of hours in the office during the dark winter days longing for the sun light and turquoise waters I have not lost my motivation to this work.

Doing this thesis has not always felt like work and sometimes I have forgotten that I am actually educating myself. Almost insidiously, during these years, I have become much more self-confident and aware of my strengths and weaknesses. In the end I understand how much I have learned about rivers, different methods, research, people, communication, writing, time management, self-discipline, self-criticism and how to handle with criticism from other researchers. In retrospect, writing the first paper was a huge effort compared to the forth one. Despite my own effort and progress, I would never have been able to finish this work without the network which has surrounded me and I want to thank those people who have assisted, supported and encouraged me on the way.

First of all I want to thank my supervisors Adjunct Prof. Petteri Alho and Prof. Hannu Hyyppä. Special thanks to Pete who has given me the most important guidance and believed in my success despite many complications on the way. It has always been easy for me to talk to you about anything; a thing that has been very valuable during this Ph.D. work and that I appreciate a lot. Maybe weeks in a small hut near the North Pole automatically breaks some barriers between people. Thanks belong to the whole Fluvial Research Group and all those colleagues who I have spent hours with in the cold rivers of Lapland during the beautiful autumn and never ending spring days and who I have written papers with: Eliisa Lotsari, Claude Flener, Leena Laamanen, Jenni-Mari Vesakoski, Yunsheng Wang, Mikel Calle, Matti Vaaja, Harri Kaartinen, Antero Kukko, Anttoni Jaakkola, Matti Kurkela, Juha Hyyppä, Saija Koljonen, Timo Huttula and the all of the people from the Finnish Geodetic Institute , Aalto University and Finnish Environment Institute who have contributed to this work in different ways. It has been great fun! I hope our co-operation will continue in the future. Thanks also to the personnel of the Kevo Research Institute and the Game and Fisheries Research (Tana River Station). The truth is that I would never have been able to produce this thesis without you all.

Thanks for Claude for being the most faithful roomie for almost 6 years, I hope I will find someone who is as intelligent (I can always ask your help) and as polite (I really appreciate the industrial peace that prevails in the office) as you are to replace you (Jenni, you are not bad either!). Jenni, I hope our co-operations is only in the beginning still. Thanks for Leena for all those jolly conversations we have had in the university and outside of it and also for your priceless work contribution. Special thanks to Eliisa. You have been a good friend and at the same time an irreplaceable colleague and advisor. Working trips with you have never been boring or foreseeable. I am glad that the distance has not affected much on our friendship. I am sure we will make a good team in the future as well!

Thanks belong also to all of the colleagues at the Geography Division, who make this a pleasant place to work. Special thanks to the professors in the physical geography, Risto Kalliola and Jukka Käyhkö for being such talented and inspiring teachers during the studies at the university level. Thanks for Leena Laurila, Annukka Malmsten and Kirsi Kunnas for helping out in many practical issues. The importance of the fellow Ph.D. students (and project researchers) is not to be sneezed either: Claude, Eliisa, Hanna, Hanna, Jenni, Joni, Juuso, Katri, Lauri, Matti, Mika, Niko, Nora, Paulina, Rebecca, Riina, Timo and many others. It is

important to have people around who share the same problems. Thanks also for sharing so many cheerful moments. You all earn special thanks for making the atmosphere of the department so inspiring, lively and comfortable!

Thanks also belong to the reviewers of this thesis, professors Stephen Darby and Stuart Lane. Your constructive feedback improved the thesis but also gave me important self-confidence.

Maija, Iisa and Eeva, it is a lot of fun to gather together from all over the Finland every now and then. Those gatherings always remind me why we became such good friends during our studies. Even though we may not have been the most tidy, decent or well-behaved students, we are after all doing quite OK, I think.

I also want to thank all my friends from outside of the university life. Annika, Anssi, Heidi, Jenni, Laura, Liisa, Pauliina, Suvi,Vivi…you make my life so fun, enjoyable and unserious, which is a perfect counterbalance to the office work. Thanks for RLP. Kaisa and Tuuli P, thanks for being friends who I never have to be afraid of losing, even if I have been too busy to keep touch. Kaisa, your talent for being able to simultaneously take things seriously and produce outrageous humour makes me feel myself privileged to have a fried like you. Tuuli P, your care-free attitude is enviable; I have done my best to absorb some of it. Thanks also for letting me offload everything onto you during these years. Tuuli E, I don't know where I would have spent all my student loan without you. I am very grateful that we found each others and explored the world together, mission is not completed.

My sister Anna-Maija deserves very special thanks. I believe that I would not have overcome the difficulties and tragedies in my (our) life, which emerged during this Ph.D., without your existence and support. There is just no one else on this world who would understand me as well as you do, which makes our hours lasting conversations extremely important to me. I also want to thank Samu, who has sympathetically allowed us these opportunities to thrash out the world, which have sometimes required lots of time and red wine. You have also given me many reasons for laughter.

I am very grateful for my mother and late father for letting me find my own enthusiasms and views without trying to direct me. I have never felt any kind of pressure from your side. Mom, I have certainly felt that no matter what I choose or decide it will receive your understanding. It is relieving that I do not have to talk about my work with you but we can concentrate on the colors of your living room`s pillows. I also want to thank you for being such a great grandma for Veikko and for taking care of him when needed. I am grateful for my father who reminded me to enjoy life and supported to go for things that I really like, not to take things for granted, and most importantly, not to take life too seriously.

Finally, I want to direct my dearest thanks to Aleksi. I may not have brought work home concretely or spent everlasting days at the university, but the work pressure and the consequent bad mood have certainly required lots of understanding and patience form you. Thanks also for your honest encouragement during this work. You took care of Veikko at home while I was finishing my Ph.D., making it possible for me to concentrate on work and not needing to worry about how things are going at home. I am also very grateful for Veikko for remaining me about what is in the end important in life. I love both of you.

LIST OF ORIGINAL PUBLICATIONS

This thesis consists of an abstract, summary and the following four papers. The papers are referred with Roman numerals:

I Kasvi E, Vaaja M, Alho P, Hyyppä H, Hyyppä J, Kaartinen H, Kukko A. 2013. Morphological changes on meander point bars associated with flow structure at different discharges. Earth Surface Processes and Landforms 38: 577-590.

II Kasvi E, Alho P, Lotsari E, Wang Y, Kukko A, Hyyppä H, Hyyppä J. *In press*. Two-dimensional and three-dimensional computational models in hydrodynamic and morphodynamic reconstructions of a river bend: sensitivity and functionality. Hydrological Processes.

III Kasvi E, Alho P, Vaaja M, Hyyppä H, Hyyppä J. 2013. Spatial and temporal distribution of fluvio-morphological processes on a meander point bar during a flood event. Hydrology Research 44: 1022-1039.

IV Kasvi E, Vaaja M, Kaartinen H, Kukko A, Jaakkola A, Alho P, Flener C, Hyyppä H, Hyyppä J. Sub-bend scale flow-sediment interaction of meander bends -a combined approach of field observations, CFD and close-range remote sensing. Submitted to Geomorphology.

Papers I and II are reprinted original publications. Paper III is reprinted in a form of authors proof. Paper IV is submitted and revised. All published articles are reprinted with the permission of the respective publisher.

CONTENTS

1 INTRODUCTION

Rivers are formed as a result of a complex interaction of water, sediment particles and gravitational forces. As the fluid and gravitational forces affect differently the particles of different size and position, erosional and depositional patterns are developed along the river channel leading to the emergence of bedforms, pools and bars, and ultimately different river channel patterns. Most commonly, the natural river channel patterns are divided into two categories, which are meandering and braiding, as straight rivers are extremely rare in nature. The early contributions of fluvial geomorphology date back to the 19th century when, based on observations of present landforms and processes as well as physical experiments, the first hypothesis and theories were outlined (e.g. Playfair, 1802; Powell, 1875; Manning, 1891; Gilbert, 1914). Many fluvial geomorphologists, inspired by physicists and chemists, were focussing on finding physical principles that would be universally applicable in explaining the different channel patterns, meandering and braiding (e.g. Jefferson, 1902; Inglis, 1937; Chitale, 1973; Parker, 1976; Chang, 1979). In meandering rivers, bends with different amplitudes and radii of curvature form a continuous sinuous channel. A point bar is usually formed on the inner bank, while the outer bank side is deep. Braided rivers, on the other hand, are characterised by alluvial islands and central bars that split the channel into two or more anastomosing, flanking channels (Leopold and Wolman, 1957). Leopold and Wolman (1957) found that the meander wavelength correlates with the bankfull discharge and channel width, while Schumm and Khan (1972) found a correlation between sinuosity and valley slope. Ackers and Charlton (1970) related the meander wavelength with discharge magnitude. In general, the peak discharges, flow velocities, slope and width-depth ratios, stream power and bed shear stresses are smaller in meandering rivers compared to braiding rivers (Leopold and Wolman, 1957; Parker, 1976; Schumm, 1985; Ferguson, 1987; Kleinhans and van den Berg, 2011).

This thesis focuses on sand-bed meandering rivers. A wide range of studies concerning meandering river processes and evolution were published already during the early 20th century (e.g. Davis, 1902; Jefferson, 1902; Inglis, 1937; Mockmore, 1944; Friedkin, 1945), and important conceptual models of the meander evolution were established (e.g. Wolman and Leopold, 1957; Leopold *et al*., 1964; Brice, 1974; Hickin, 1974). For long, meander development was hypothesised to stabilise after the evolution was complete (e.g. Leopold and Wolman, 1957; Leopold and Langbein, 1966; Ackers and Charlton, 1970; Schumm and Khan, 1972). In the 1970s and 1980s, many important field-based studies increasing the understanding of complex processes of meandering rivers, such as secondary circulation and sediment transport patterns, were published (e.g. Hooke, 1975; Jackson, 1975; Bridge and Jarvis, 1976; Bathurst *et al*., 1977; Bluck, 1982; Dietrich and Smith, 1983, 1984; Thompson, 1986). These studies were based on empirical measurements of the fluvio-morphological characteristics of the rivers. For example Dietrich and Smith (1983, 1984) measured the three dimensional flow structures and their implications to sediment transport patterns in a field environment with high detail by designing a functional measurement campaign. These studies provided a strong basis for the understanding of the complex processes of meander bends. Since those studies, the understanding of the fundamental mechanics of meander bends has not developed or been challenged notably.

However, the development of empirical measurement techniques during the late 20th and early 21st centuries, especially the close-range remote sensing techniques, enabled riverine investigations with higher spatial and temporal resolution than before and therefore inspection of phenomenon that had earlier been beyond the capacity of the measurement technologies (e.g. Ferguson *et al*., 2003; Frothingham and Rhoads, 2003; Milan *et al*., 2007; Hooke, 2008; Gautier *et al*., 2010; Hooke and Yorke, 2010; Engel and Rhoads, 2012). Even

though many fluvio-morphological processes, generic for meandering rivers, were observed in those studies (Ferguson *et al*., 2003; Frothingham and Rhoads, 2003; Engel and Rhoads, 2012) they also highlighted that the meandering rivers are complex systems with nonlinear and unique behaviour (Gautier *et al*., 2010; Hooke and Yorke, 2011; Hooke, 2007a). During the late 20th century, also the use of computational fluid dynamics (CFD), which enables spatial and temporal resolution of flow and sediment transport data impossible to achieve with field measurements, became a standard approach in fluvial geomorphology (e.g. Ikeda *et al*., 1987; Shimizu *et al*., 1990; Ferguson *et al*., 2003; Lane *et al*., 2007; Alho *et al*., 2010; Kleinhans, 2010; Güneralp and Martson, 2012). More recently, mathematical models also have been used in assessment and development of theories of meandering behaviour, challenging the field and laboratory experiments in investigating natural processes (e.g. Booker *et al*. 2001; Ferguson *et al*., 2003; Duan and Julien, 2005). Thus, the new research questions of fluvial geomorphology have moved closer to those of the early 20th century with an attempt to create and improve widely applicable physical laws and quantitative expressions (Wohl, 2014). Still, many processes and phenomena are beyond the measurement techniques' capacity today and can only be approached implicitly. Also, computational models, which are always simplifications of the real world, have their deficiencies, such as sub-grid scale processes, which cannot be modelled but have to be parameterised. Sediment sorting and transport are the main challenges of computational modelling in the second decade of the 21st century. Therefore, in fluvial geomorphology, it has become increasingly popular and supported to combine various study approaches simultaneously, i.e. empirical observations and modelling, as they represent nature in different ways and the deficiencies of one approach can be compensated by others (e.g. Darby *et al*., 2002; Lane *et al*., 2007; Casas *et al*., 2010; Kleinhans, 2010; Güneralp and Martson, 2012; Ottevanger *et al*., 2012; Lotsari *et al*., 2014a).

The full potential of the new methodological approaches, including close-range remote sensing techniques and computational fluid dynamics, has not yet, however, been fully exploited in deriving new understanding in fluvial geomorphology, neither have their functionality and sensitivity been assessed in an applied purpose in a sand-bed meandering river. It can be hypothesized that the increased spatial and temporal resolution achieved by combining conventional field measurements with a range of modern technologies will provide new insights to the spatial patterns of the flow-sediment interaction in meandering streams, which have perceived to show notable variation in space and time.

In this thesis, the processes of a sand-bed meandering river are approached by combining existing theories, empirical methods and computational modelling of flow and morphology (Fig. 1). The main aim of this thesis is to combine and assess the conventional field measurements, close-range remote sensing and computational fluid dynamics in order to improve the spatial and temporal resolution of the fluvio-geomorphological data and, by exploiting this methodological approach, to increase the scientific understanding of fluvio-morphological processes on sand-bed meandering rivers. The following research questions are addressed: How are the fluvio-morphological processes distributed in sand-bed meander bends in space and time? What are the factors influencing the spatial patterns of flow-sediment interaction over a sandy meander bend? What kinds of new perspectives can the exploited study approaches provide to fluvial geomorphology of meander bends? What are the challenges and shortages of the used methodological approaches and the remaining gaps in the data gathering and understanding of the fluvio-morphology of meander bends?

The study is realised in Sub-Arctic Finland, in a meandering, unregulated River Pulmanki. The channel is sand-bedded and mobile, and it is under continuous morphological change with limitless sediment sources. Normally, one significant flood event, a snow-melt-induced spring flood, occurs annually, which is typical for Arctic and

sub-Arctic rivers. The following objectives have been drawn in order to answer the research questions (Fig 1):

a) To demonstrate and assess:
   -study approaches combining conventional field measurements, close-range remote sensing and computational fluid dynamics (all papers)
   -the sensitivity and functionality of hydro- and morphodynamic models in natural meandering river environment (paper II).
b) To derive new insights to the spatial and temporal patterns of sub-bend scale fluvio-morphological processes over sand-bed meander bends based on the demonstrated study approaches (papers I, III, IV).
c) To analyze the factors influencing the spatial patterns of flow-sediment interaction over a sandy meander bend (papers I, III, IV)

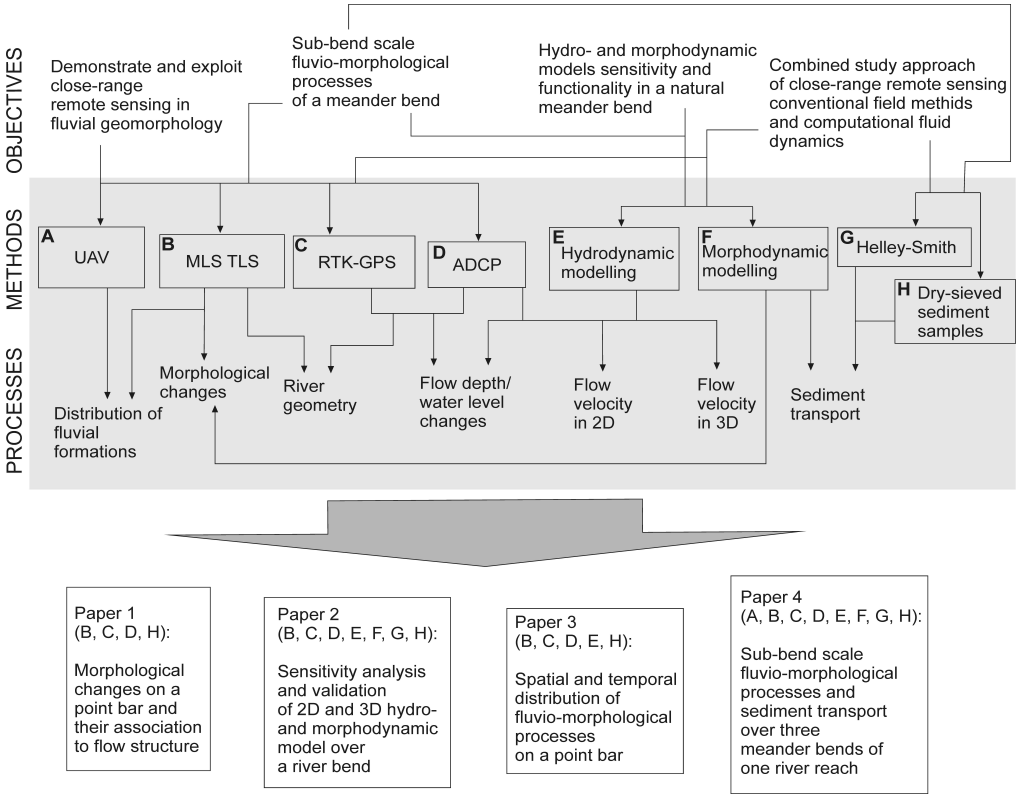

Fig. 1. The study approach of the thesis. The objectives are located at the top of the figure. The framework of the methodology (A-H) and measured processes are in the grey box. The main outcomes of the thesis are presented in four papers, which are shortly described at the bottom of the figure within the white boxes. The methodological approaches (A-H) of each paper are marked inside the boxes. For simplicity, some interconnections of the methods have been left out of the figure; for example the RTK-GPS was exploited to locate many of the other measurements. Further, the remote sensing based data and sediment samples were used to build the computational models.

Paper I presents a field-based study of the morphological changes over two meander point bars and their association to the 3D flow structure of three different discharges during a flood event. The morphological changes are mapped with high accuracy using terrestrial and

mobile laser scanning (TLS and MLS, respectively). The 3D flow structure over the bends is measured using an ADCP. The dominant processes and controlling factors over different parts of the bends and the role of the 3D flow structures are analysed based on state-of-the-art field measurements.

Paper II focusses on the sensitivity and functionality of hydro- and morphodynamic models in river bend. The 3D flow structures, curved shape of the channel and transverse differences in bed level cause several challenges for the mathematical modelling of processes in meandering rivers. In natural environments, many unpredictable factors are present, making the modelling of natural rivers demanding. Further, many processes are adjusted or controlled by user-defined parameters in the simulation approaches, and thereby the selection of the parameters influences the model outcome. In this study, the models' sensitivity to various user-defined parameters (grain size distribution, roughness, transverse bed slope effect, secondary flow and sediment transport relation) is asnalysed in a meandering river environment. In addition, 2D and 3D hydro- and morphodynamic models are compared with detailed field measurements (TLS, MLS, ADCP-based flow structure) to assess the model functionality in a natural meander bend.

In paper III, a combined approach of detailed field measurements and a 2D hydrodynamic model is used to study the spatial and temporal distribution of sub-bend scale fluvio-morphological processes of a meander bend. Even though many fluvial and morphological processes are known to occur generally on meander point bars, the role of the flood magnitude and the duration of different phases of the flood to the morphological changes over point bars have not been studied extensively. In this study, the TLS and MLS approaches provide detailed change detection data of a meander point bar, and the hydrodynamic model enables the analysis of the temporal occurrence of flow characteristics and erosional and depositional processes over the point bar.

Paper IV represents a study of fluvio-morphological processes over three meander beds during a flood event. A study approach exploiting a combination of field survey, close-range remote sensing and computational fluid dynamics (CFD) information of flow and sediment transport was applied. The geometry of the CFD data is based on MLS, TLS and sonar. The interpretation of the fluvial formations over the point bars is improved using UAV-based aerial photography (grid resolution of 0.05 m). The pre- and post-flood grain size distribution (GSD) data is used to further explain the processes. The hydrodynamic model with sediment transport provides spatially and temporally extensive information of the fluvio-morphological processes and enables the examination of sediment movement during a flood and the estimation of the temporal occurrence of bed-level changes.

2 BACKGROUND

2.1 Fluvial geomorphology: processes and terminology

Due to the importance of rivers for human societies as water and food suppliers and transport routes, fluvial geomorphology has been a focus of scientific research for a long time. Thus, many fundamental terms, theories and equations were developed before the 21st century. As the flowing water in an open channel is affected by gravity and friction, the potential energy of the water is converted to kinetic energy of the water and transported particles and dissipates. Many factors affect the channel development, such as the soil type, sediment size and availability, channel geometry, internal friction of the water, the friction of the channel boundaries and the slope. The internal friction can be quantified using the concept of viscosity, which describes the resistance of the fluid to its motion. Molecular viscosity is the internal viscosity of the water, which resists flowing. The ratio of molecular viscosity and fluid density is called kinematic viscosity (Fox and McDonald, 1978) (V_k, m^2 s^{-1}). With increasing water temperature, the molecular and kinematic viscosity decrease. Eddy viscosity (V, m^2 s^{-1}), by contrast, is a result of turbulent fluctuations in the flow; it describes the vertical and horizontal transport and dissipation of energy (Robert, 2003). Turbulence may have an important impact on the processes in the river, as it also affects the sediment transport, especially in san-bed channels, and allows the mixing of dissolved material and particles vertically and horizontally in the water. In laminar flow, the water flows in parallel layers, and no transfer of momentum or mixing between the layers occurs.

The friction between the water and the channel boundaries leads to movement of the sediment particles and evolution of the river. The resistance of the river bed to the flowing water can be expressed using bed shear stress (N m^{-2}), which has been widely used in fluvial geomorphology to determine the flow-channel interaction. A simple and widely used way to calculate the bed shear stress is using the following formula (e.g. Bathurst *et al*., 1979; Andrews, 1980; Baker and Costa, 1987; Magilligan, 1992; Rüther *et al*., 2010):

$$T = \rho g D S \qquad \text{Equation 1}$$

where ρ is the density of water (kg m^{-3}), g is the gravitational acceleration (m s^{-2}), D is the flow depth (m) and S is the slope. Stream power is used to describe the rate of energy dissipation of water against the channel bed. The so-called total stream power (W m^{-1}) (e.g. Reinfelds *et al*., 2004; Barker *et al*., 2009) can be calculated based on discharge and stream slope as follows (Bagnold, 1966):

$$SP = \rho g Q S \qquad \text{Equation 2}$$

where Q is the flow discharge (m^3 s^{-1}). Another form of stream power, i.e. the unit stream power, was later created to better describe the spatial variation of stream power within a channel. In the unit stream power (W m^{-2}), the discharge is replaced by separate terms of flow velocity (m s^{-1}) and depth (m). The unit stream power is the rate of energy dissipation of water against the channel bed per unit area and is calculated as follows (Bull, 1979):

$$\omega = \rho g D S v \qquad \text{Equation 3}$$

where v is the flow velocity. The unit stream power has been used by many researchers to analyse the energy dissipation of flow and its spatial variation over a channel (Baker and Costa, 1987; Lewin and Brewer, 2001). The bed shear stress and stream power are strongly

related to the sediment transport capacity of the stream flow, and the flow velocity is very sensitive to the frictional forces. Thus, critical thresholds for initiation of sediment movement of different sizes of particles have been defined based on the flow parameters. Thresholds based on flow velocity (e.g. Hjulström, 1935; Rouse, 1937), bed shear stress (e.g. Shields, 1936) and stream power (Bagnold, 1966, 1980) for the initiation of motion of different particle sizes were developed, and the relations led to the development of sediment transport algorithms (e.g. Einstein, 1942, 1950; Meyer-Peter and Müller, 1948; Bagnold, 1966, 1980; Engelund and Hansen, 1967; van Rijn, 1984a,b).

One of the simplest transport algorithms still in use (e.g. Hèquette *et al*., 2008; Wu *et al*., 2008; Bolle *et al*., 2010; Schuurman *et al*., 2013) was developed by Engelund and Hansen (1967). The formula does not separate suspended load and bed load. However, especially in sand-bed rivers, finer sediments are lifted into suspension and larger grains move as bed load by rolling or sliding, specific algorithms were also established for bed load and suspended load transport (e.g. van Rijn, 1984a, b). Thus, the algorithms were developed further to cover also mixed grain size distributions, for example (Bagnold, 1980; van Rijn, 1993). Amongst the widely used sediment transport algorithms, that of van Rijn (1993) is the most physics-based (Pinto *et al*., 2006).

Based on the sediment transport algorithms, which includes the initiation of motion as well as particle settling, the changes in the bed material can be calculated. The algorithms are simplifications of the real sediment transport, as many unpredictable factors, such as sediment supply from upstream (cf. Lane *et al*., 1996), run-off, vegetation and other biological factors affect the actual transport rate, but they provide valuable new insights to the flow-sediment interaction.

The spatial and temporal variation of the flow characteristics and grain sizes causes variation in the distribution and form of erosion and deposition. As a consequence of the flow-sediment interaction, different formations are developed. The riverine sedimentary formations can be divided into *meso-, macro- and microforms* according to their size (e.g. Jackson, 1975; Kennedy, 1969; Engelund and Fredsöe, 1982). *Mesoforms* include floodplains and channels, while the term *macroform* refers to relatively large, sub-channel scale formations, such as point bars, scroll bars and side bars. *Microforms* include rippels and dunes, for example. The incision, development and required circumstances of these formations have been a focus of many studies, and the developments in the measurement technologies have led to ‘a new wave’ of bed form studies (e.g. Bennett and Best, 1995; Carling *et al*., 2000; Seminara, 2010; Nelson *et al*., 2011; Coleman and Nikora, 2011). On a more general scale, the magnitude and frequency of the flow discharge and the sediment supply fluctuations from upstream have been noted to be the major controls of sediment transport and the morphological changes in rivers (e.g. Carling and Beven, 1989; Ferguson, 1994; Lane *et al*., 1996).

2.2 Progress in empirical study approaches of fluvial geomorphology

In this chapter, the progress in those empirical study approaches that have been used in fluvial geomorphology and are related to the current work is introduced briefly. Thus, many study approaches and methods, geochronological studies and laboratory experiments, for example, are not covered in this chapter but have nevertheless had a notable contribution in the development of fluvial geomorphology. Empirical approaches include both conventional field methods and more modern remote sensing techniques.

The studies in fluvial geomorphology during the early 20th century were based on empirical observations in the field (e.g. Lane, 1935) and on laboratory experiments (e.g. Gilbert, 1914; Friedkin, 1945; Schumm and Khan, 1972; Hooke, 1975). The flow velocity

was measured in one dimension using a mechanical current meter, and the discharge calculation was based on the velocity measurements. The measurement of the river geometry (both topography and bathymetry) was realised along cross-sections over the river, the locations of which depended on the research question (Bridge and Jarvis, 1976; Dietrich and Smith, 1983; Ferguson and Ashworth, 1992; Warburton *et al*., 1993). Common methods to determine the differences of elevation between the points along a cross-section were levelling (see Bitelli *et al*., 2000) and theodolite (e.g. Low, 1952; Ritchie *et al*., 1988), which were used widely during the 20th century.

The increasing availability of aerial photographs since the beginning of the 20th century encouraged photogrammetric surveys and an increasing amount of statistical studies determining the geometrical characteristics of the river channel patterns (Tieje, 1929; Smith, 1941; Ray, 1960; Schumm, 1963; Brice, 1974). However, still during 1970s and 1980s the photogrammetric surveys were expensive and challenging to realize due to the precise requirements for image and camera orientation and the expensive analogue plotters needed for the post-processing (cf. Statham, 1990). Since critical developments in analytical photogrammetry in during 1980s, the airborne surveying became more popular in creating topographical maps also in fluvial geomorphology. It became possible to deal with oblique images and to use relatively cheap non-metric cameras and soon the images were processed and analysed mostly using computers (e.g Lane *et al*., 1992). Thus, during 1990s aerial photography became involved in DEM based topographical surveys of rivers (e.g. Lane *et al*., 1994). Since then, the airborne techniques have been exploited in a wide range of research subjects among fluvial geomorphologists, from bathymetric surveys (Winterbottom and Gilvear, 1997; Bryant and Gilvear, 1999; Williams *et al*., 2014) to grain-scale characterisations of the rivers (Carbonneau *et al*., 2004; Dugdale *et al*., 2010). In addition, the digital photogrammetry facilitated the use of ground based oblique photographs in geomorphological studies (Chandler *et al*., 2002). The main advantages of photogrammetry are that it enables access to areas that are remote and difficult to reach (Dean and Morrissey, 1988; Duncan *et al*., 1998) and enables surveys over extensive areas (Westaway *et al*., 2003). Recently, the unmanned aerial vehicles (UAV) also have become increasingly used in collecting high-resolution digital images, but their application in fluvial geomorphology has thus far been limited (Lejot *et al*., 2007; Flener *et al*., 2012). The biggest advantages of the UAV technique are the cost efficiency and very high data resolution compared to traditional aerial photographs.

Despite methodological achievements in fluvial geomorphology, measuring the bed load transport remains problematic still today. Bed load is difficult to measure, because, for example, catching the real variability of bed load requires a large number of samples because bed load transport varies a lot in space and time and the presence of a sampler on the river bed disturbs the flow and sediment transport characteristics nearby (Gomez, 1983; Rennie *et al*., 2002). Important achievements among the sediment transport measurement techniques occurred during the 1970s (Wohl, 2014). These include pressure-difference bed load samplers, for example (Helley and Smith, 1971), and acoustic and optical backscattering techniques to measure the suspended sediment (Gray and Gartner, 2009). The pressure-difference samplers were designed so that the velocity of the flow entering the device and the surrounding flow velocity are equal, as the samplers walls diverge towards the rea creating a pressure drop at the sampler exit. Sediment is retained in ta mesh bag mounted behind the sampler. Even though bed load measurement techniques, which improved the spatial and temporal resolution of the measurements, were developed during the 1980s (e.g. Reid *et al*., 1980, Birkbeck bedload sampler), the simple Helley-Smith sampler has been widely used until today (Ashworth and Ferguson, 1986; Lane, 1996; Ryan *et al*., 2005; Rathburn *et al*., 2013). However, various factors affect the measurement result gained with the Helley-Smith

sampler (cf. Gomez and Troutman, 1997). As the sampler touches or even shovels into the river bed in the beginning of the measurement, especially in a sand-bed rivers, it results to an over catch (Gomez *et al*., 1990; Gaweesh and van Rijn, 1994; Lotsari *et al*., 2014a). Further, as the aperture of the device is normally 152 mm in height, it measures also other than bed load, as all the material moving immediately above the bed is collected (Einstein, 1948). So called sampling efficiency, defined as the ratio of the measured bed load to the actual bed load (Hubbel, 1964) has been used to describe the correctness of the measurement and previous studies have shown varying results regarding to the sampling efficiency of the Helley-Smith sampler (Emmett, 1980; Hubbel *et al*., 1981; Glysson, 1993). However, the level of the bed load measurement accuracy of Helley-Smith sampler is competitive compared to other available measurement techniques and the problems with the measurement uncertainties are more related to the poor sampling techniques and the problems to catch the spatial and temporal variation of the transport (Gomez *et al*., 1991).

Before 1990s, the flow velocity measurements were based on propeller type, and, after 1970s the electromagnetic current meters (e.g. Bathurst *et al*., 1977). With the emergence of the acoustic measurement technologies (e.g. acoustic Doppler velocimeters (ADV) and acoustic Doppler current profilers (ADCP)) the three-dimensional velocity data gathering became possible (e.g. Hodskinson and Ferguson, 1998). ADV is used to measure the flow field in an individual point while ADCP can measure flow field from a moving platform. During 1990s, only the ADVs were used to measure the 3D flow fields in shallow rivers (e.g. Voulgaris and Trowbridge, 1998) while the use of ADCPs was limited to deep rivers because of the large blanking depth and poor vertical resolution (e.g. Simpson *et al*., 1990). The acoustic techniques are based on the Doppler effect of transmitted sound waves, which are scattered from small particles in the water column. The sensor transmits a sound pulse with a certain frequency, and the backscattered sound is affected by the Doppler shift, because the particles are moving in the water relative to the device (Gordon, 1996). The flow velocity is calculated based on the velocity of the particles relative to the sensor, while the sensor records its own velocity relative to the river bed. Since then the acoustic technologies have been developed and the ADCP can nowadays be applied in shallow waters as well. This has led to an emergence of a wide range of studies exploiting ADCP and dealing with flow structure, turbulence and its changes in different circumstances (Dinehart and Burau, 2005a; Nystrom *et al*., 2007; Rennie and Church, 2010; Claude *et al*., 2014). Thus far, the ADCP based flow field measurements have been mostly carried out along a series of river transects (e.g. Dinehart and Burau, 2005a; Williams *et al*., 2013). The discharge can be measured using an ADCP by moving the device perpendicularly across the river. The frequencies used range from ~70 kHz to several megahertz (Gordon, 1996; Sontek/YSI, 2010). The lower frequencies are used in deep waters. Thus, devices with multiple frequencies enable measurements in shallow and deep areas. Today, ADCP devices do not measure the flow velocities at distances less than 0.2 m from the river bed (side lobe interference) or the water surface (blanking distance) (cf. Yorke and Oberg, 2002).

The echo sounding techniques became widely used in scientific bathymetric measurements during the latter half of the 20th century (Dost and Mannaerts, 2008). The working principle of an echo sounder remains that of an ADCP. A transducer, which is placed on the water surface, sends a sound wave to the target (e.g. river bed), and the sound wave is reflected back from the target. The depth of the water column is calculated based on the travelling time of the sound wave. Nowadays, very high resolution and efficient devices with multiple beams are used in detailed fluvio-morphological surveys (e.g. Parsons *et al*., 2005; Laustrup *et al*., 2007; Kaeser *et al*., 2013). Typically, the achieved point spacing is more than 0.2 m (cf. Parsons *et al*., 2005). The frequencies of the sound pulses used in

riverine environments range from 200 kHz to 1 MHz (Parsons *et al*., 2005; Sontek/YSI, 2010; Kaeser *et al*., 2013). Lower measurement frequencies are used in deep waters.

The use of geographical information systems (GIS) became common during the 1980s and 1990s, enabling new kinds of spatial analyses and spatial data management. One of the most important improvements linked to GIS is the gathering and management of spatially covered topographic and bathymetric data and the construction of the digital elevation model (DEM). The DEMs have markedly improved the observations of the formations, changes and processes of fluvial environments (e.g. Brasington *et al*., 2000). By subtracting DEMs of different occasions, i.e. creating a DEM of difference (DoD), it is possible to determine the volume of erosion and deposition on the surveyed area between the two surveys (e.g. Lane *et al*., 1996; Brasington *et al*., 2003; Wheaton *et al*., 2010). DEMs also provide the topographic boundary data for higher order (i.e. 2D and 3D) computational fluid dynamics (e.g. Horrittt and Bates, 2002). First, the DEMs applied in fluvial geomorphology were based on, for example, ground-based or aerial photogrammetry or theodolite and total station measurements (e.g. Lane *et al*., 1996; Butler *et al*., 1998; Heritage *et al*., 1998; Kleim *et al*., 1999; Chappell *et al*., 2003; Fuller *et al*., 2003; Mottershead *et al*., 2008). With these methods, however the measurements were mostly limited in measuring a small area in detail or a large area with low spatial resolution (Heritage and Hetherington, 2007; Large and Heritage, 2009) although the photogrammetric methods provided improvement to this problem (Lane *et al*., 2003; Westaway *et al*., 2013).

At the same time, the developments in the satellite navigation systems changed the culture of geometric data positioning, making the data gathering faster and improving the positional accuracies and thereby boosting the shift from cross-sectional to aerial surveys (e.g. Dunbar *et al*., 1999; Brasington *et al*., 2000). The drop in prices and improved functionality of the global navigation satellite system (GNSS) facilitated the definition of the spatial reference of the topographic and bathymetric measurements and thereby DEM generation (Brasington *et al*., 2003; Kaplan, 2006). The GNSS includes NAVSTAR global positioning system (GPS) and GLONASS and enables fast and accurate definition of the horizontal and vertical location of a survey point. A moving GNSS device receives radio wave signals from satellites orbiting the earth. The signals carry information about the distance between the device and the satellites, and the location of the device on earth can be calculated based on that (Oguchi *et al*., 2011). At least four satellites are needed to calculate a 3D position. Because the standard GPS system only allows for a positional accuracy of ~10 metres, various methods have been developed to enhance the accuracy. In the differential GNSS (DGNSS) system, an accurate location of a reference station is known, and thus the difference between the correct and the measured position of the reference station can be calculated and the correction vector defined based on that (e.g. Farrell and Givargis, 2000). The correction vector is then used to correct the survey point measured by the user. A positional accuracy of ~1 m can be achieved using a DGNSS system. To improve the measurement accuracy further, a real time kinematic GNSS (RTK-GNSS), which is a further developed differential GNSS, can be used (Edwards *et al*., 1999; Hu *et al*., 2003). With at least 5 common satellites between the moving device and the base station, an accuracy of few centimetres can be achieved in real time (Bilker *et al*., 2001; Morales and Tsubouchi, 2007). The correction signal for a RTK-GNSS can also be received from a virtual reference station (VRS) network (Vollath, 2000; Rizos, 2002). The virtual reference stations are linked to a control centre, which provides spatially varying correction over the network. The moving GNSS device receives the correction signals from the virtual station similarly as from a real reference station, reaching an accuracy of less than 5 cm (Landau *et al*., 2002; Retscher, 2002). The VRS network also increases the flexibility in data correction, as the area is not restricted by the location of the reference station (Gao *et al*., 1997).

During the first two decades of the 21st century, the light detection and ranging (LiDAR) applications have increased markedly, providing improved and more effective solutions to geomorphological mapping of fluvial environments (e.g. Charlton *et al*., 2003; Thoma *et al*., 2005; Heritage and Hetherington, 2007; Notebaert *et al*., 2009; Rhoades *et al*., 2009; Hohenthal *et al*., 2011; Stott, 2013). The LiDAR technique is based on an active instrument that emits and receives laser light. The laser light, originally called 'light amplification by stimulated emission of radiation', is actively stimulated coherent light, meaning that all the light waves have the same wavelength and frequency. The LiDAR measurement can be based on the time of flight (TOF) of the laser pulse or the phase-shift of a continuous laser wave (Petrie and Toth, 2009). A TOF instrument calculates the distance of a target from the device based on the travelling time of a short but intense laser pulse to the target and back (Distance = speed of light x time of flight/2). The phase-shift instrument transmits a continuous laser beam and calculates the distance between the scanner and the target based on the known wavelength (L) of the pulse and the phase difference of the emitted and transmitted laser beam (Distance=(nL + ΔL)/2). The main advantages of the LiDAR techniques are the accuracy and very high speed of data collection (Hodgetts, 2009).

The laser scanning can be realised from an aircraft, i.e. airborne laser scanning (ALS) or from the ground, i.e. terrestrial laser scanning (TLS). Together with the high accuracy GPS, the ALS enables the gathering of detailed geometric data of rivers substantially faster than the conventional methods (Petzold *et al*., 1999). ALS works well in surveys of large areas, and point densities of 5–50 points/m^2 and accuracies of 0.10 m to 0.5 m can be achieved (e.g. Heritage and Hetherington, 2007; Höfle *et al*., 2009; Vosselman and Maas, 2010). However, it does not allow for detailed geomorphological surveys. In that case, a TLS can be applied. It further enhances the ability to realise very detailed surveys (Hodge *et al*., 2009; Heritage and Milan, 2009). TLS surveys are realised by placing the laser scanner on a tripod close to the scanning target. Typically, infrared wavelengths from 700 nm to 1500 nm are used in TLS, and the modern devices are able to measure approximately one million points per second with distance measurement accuracy of a few millimetres (e.g. Faro, 2014; Leica Geosystems, 2014). Due to the very high accuracy and spatial resolution of the TLS, it has had a notable influence in the development of fluvial geomorphology in enabling very detailed observations of fluvial formations, for example (Hodge *et al*., 2009; Williams *et al*., 2014), morphological changes (Milan *et al*., 2007; Pizzuto *et al*., 2010) and grain size and roughness (Heritage and Milan, 2009).

The TLS surveys are, however, rather time consuming as only relatively small areas can be scanned once with high detail (Alho *et al*., 2009a; Williams *et al*., 2014). Mobile laser scanning (MLS) has been developed to overcome this shortage (e.g. Kukko *et al*., 2007; Hyyppä *et al*., 2009). In MLS, the scanner is mounted on a moving platform, such as a car (e.g. Kukko *et al*., 2009) or on a boat (e.g. Alho *et al*., 2009a), and the measured laser point cloud is geo-referred based on the simultaneous measurements of RTK-GPS and inertial measurement unit (IMU). IMU tracks the acceleration and orientation of the device with high frequency (~100 Hz) (Vaaja *et al*., 2011). The usage of MLS in fluvial geomorphology, however, has thus far been limited.

One of the main challenges for the empirical surveys is how to achieve sufficient temporal resolution to study rapidly evolving fluvial processes and forms in the required level of detail (Heritage and Hetherington, 2007; Guerrero and Lamaberti, 2011). Mostly the techniques still allow for snap-shot measurements and, considering that continuous recording would be possible in some circumstances, the spatial coverage would probably be poor. Also, the prices of certain study equipment still limit their wide usage (e.g. Williams *et al*., 2014). For example, the recent developments in photogrammetric methods and the prices of the devices are already challenging the mobile laser scanning approach in fluvial geomorphology

(cf. Micheletti *et al*. *in press*). Photogrammetric approaches have also shown high potential for closing the existing gap between the topographical and bathymetric data quality (e.g. Westaway *et al*., 2003; Flener *et al*., 2013; Williams *et al*., 2014). The future will show what will be the most feasible approach to capture the whole river channel geometry with reasonable resolution, effort and cost.

2.3 Computational fluid dynamics approaches in fluvial geomorphology

In this chapter, the term modelling refers to computational fluid dynamics, which uses the Reynolds-averaged Navier-Stokes shallow water equations (conservation of mass and momentum) to simulate movement of flow and sediment particles. The Reynolds averaging means that, as the computational grids are too coarse to resolve turbulent fluctuations, the original Navier-Stokes equations are Reynolds-averaged and introduced with additional terms, i.e. Reynolds stresses, which represent the effects of the turbulence on the mean flow. Reynolds stresses are defined using the horizontal eddy viscosity concept (cf. Prandtl, 1945). They neglect the shear stress along closed boundaries. Constant values may be defined for the eddy viscosity coefficient, or they may be computed using a turbulence closure model. The turbulence closure models have been implemented to better describe the transport of turbulence by the mean flow, in other words to overcome the limitation of a constant value approaches (Rodi, 1980; Lane, 1998). One of the most widely used turbulence models is the k-ε-model (e.g. Booker *et al*., 2001; Lesser *et al*., 2004; Rodriguez *et al*., 2004; Rüther and Olsen, 2007), which is also used in this study. It solves the transport equations for the turbulent kinetic energy k and for the energy dissipation ε (see for example Rüther and Olsen, 2007), and it does not require any empirical input (Wilson *et al*., 2003). Later, the standard k-ε-model has been modified using a renormalization group theory (RNG model) in which an extra production term for e is introduced (Yakhot and Orszag, 1986). The RNG model attempts to describe the different scales of turbulence and thereby to improve the description of turbulence further. The RNG model has been noticed to represent better complex flow structures, for example zones of separation and reattachment, compared to the standard k-ε-model (Yakhot *et al*., 1992; Lien and Leschziner, 1994; Bradbrook *et al*., 1998).

Based on the Reynolds-averaged Navier-Stokes shallow water equations, the model calculates the flow motion along the model domain for the given hydraulic conditions. The geometry of the model domain can be represented using cross-sections or a grid. The solution of the fluid equations can be further used to simulate the sediment transport and morphological changes. The main components needed to build a hydrodynamic simulation are channel geometry (grid, mesh or cross-sectional), (spatially and temporally varying) boundary conditions and the estimates of the roughness of the river bed. In the morphodynamic model, for example, the grain size distribution and sediment transport algorithm must be specified.

The equations can be resolved in 1, 2 or 3 dimensions and as steady- or unsteady-state. In this study, 2- and 3-dimensional unsteady approaches are applied, and thereby the river channel geometry is represented as a grid. Normally, structured grids are applied in CFD. In this study, two types of structured grids, i.e. rectangular and curvilinear, are used. A rectangular grid consists of equally sized and shaped rectangles, while the boundaries of a curvilinear grid follow the boundaries of the river, and the grid cells are not rectangles but quadrilateral. The curvilinear grid allows for finer grid resolution over the areas of interest and also more accurate simulation of the processes along the river boundaries. In the case of a multidimensional model, the fluid motion is resolved in each grid cell over a series of boundary conditions, which change in time. In the case of a morphodynamic model, the sediment dynamics are also computed in each grid cell based on the hydrodynamic

calculations. In 2-dimensional models, the depth-averaged flow velocity and direction is solved. In such models, the effect of the vertical flow structure may be represented by a secondary circulation sub-model, which aims to achieve the more correct estimation of the real 3D flow field (e.g. Blanckaert and de Vriend, 2003; Rodriguez *et al*., 2004; Nicholas, 2013; Schuurman *et al*., 2013). In 3-dimensional models, the vertical flow velocities and spiral flows are also solved (Lane *et al*., 1999). In a quasi-3D model, the vertical momentum equation is reduced to the hydrostatic pressure equation, following the shallow water assumption, as the vertical accelerations can be assumed to be small compared to gravitational acceleration. The quasi-3D approach enables the modelling of 3D flow structures and consequent morphodynamics to a certain level, but it is computationally much more efficient to run compared to a fully 3D model.

The sediment transport is calculated based on the solutions of the hydrodynamic equations using one of the many established equations (e.g. Engelund and Hansen, 1967; van Rijn, 1984a–c), and the bed update may be calculated based on the sediment transport in each grid cell. Also, the transportation of other elements, such as salt, heat and nutrients, can be modelled, but this is out of the scope of this research.

The hydro- and morphodynamic models have been increasingly applied by fluvial geomorphologists since the 1990s due to increased computational power and personal computers (e.g. Bridge *et al*., 1992; Hodskinson and Ferquson, 1998; Lane and Richards, 1998; Nicholas and Smith, 1999). The main advantages of the hydraulic modelling or CFD include the good spatial and temporal resolution and the possibility to simulate past or hypothetical events. Thereby, it can be exploited to, for example, test (e.g. Booker *et al*., 2001) or specify theories of fluvial geomorphology (e.g. Bradbrook *et al*., 1998; Hodskinson and Ferguson, 1998; Ferguson *et al*., 2003), model past events (e.g. Carling *et al*., 2010) and estimate future conditions (Lotsari *et al*., 2010). In all of the applications, the model is used to replace or enhance the spatial and temporal resolution of field measurements. The first models applied were one dimensional, and therefore the transverse and turbulent flow structures were not modelled. The application of two-dimensional models allowed for the examination of the spatial variation of the flow velocity and direction over a river reach, which is especially important in curved channels (e.g. Carling *et al*., 2010). This widened greatly the research questions to which the hydraulic models were applied. Two-dimensional models enabled the modelling of spatially varying flow velocities and processes, such as bank erosion (Darby *et al*., 2002) as well as meander migration (Duan *et al*., 2001). Especially in curved channels, with a highly 3-dimensional flow field, at least a 2D model with of secondary flow correction is required (e.g. Nicholas, 2013).

Even though the first 3-dimensional approaches date back to the 1990s (e.g. Shimizu *et al*., 1990; Hodskinson and Ferguson, 1998), the 1- and 2-dimensional approaches were still the most widely used at the beginning of the 21st century (Lesser *et al*., 2004). Due to the increased computational power, however, a growing amount of studies applying 3-dimensional models have been published during the first decades of the 21st century (Dargahi, 2004; Rodriguez *et al*., 2004; Rüther and Olsen, 2007; Khosronejad, 2007; Nicholas *et al*., 2012). The 3D approach is especially advantageous in modelling complicated flow fields, such as recirculation zones, which are present in meandering streams or the distribution of shear stresses over the bends (Lane *et al*., 1999; Rodriguez *et al*., 2004). Also, the improvements in the measurement techniques have enabled construction of more and more detailed simulations. For example, the interaction of spiral flow structures and riverine morphodynamics has been studied (Casas *et al*., 2010). The turbulent fluctuations are still, as mentioned above, mostly handled as sub-grid scale process and thus modelled based on semi-empirical parametrisation (e.g. Lesser *et al*., 2004; Rüther and Olsen, 2007).

Other examples of common user-defined parameters are grain size distribution and sorting, bed and bank friction, and transverse bed slope effect. The parametrisation may significantly affect the model outcome (Bates *et al*., 1998; Lane *et al*., 1999; Wilson *et al*., 2003; Horritt *et al*., 2006; Schuurman *et al*., 2013). For example, the commonly used uniform grain size value over the modelling area in sediment transport equations has been noted to lead to erroneous sediment transport and morphological change magnitudes (Nicholas, 2000; Papanicolaou *et al*., 2008; Nicholas, 2013). Also, the choice of the sediment transport algorithm has been found to have an important effect (Pinto *et al*., 2006). In addition, the quality of the boundary conditions as well as the grid resolution notably affect the modelling results (Lane *et al*., 1999; Bates *et al*., 1998; Horritt *et al*., 2006).

Thus, despite the evident advantages of CFD as a tool for fluvial geomorphologists, it should still be treated as simplified representations of real-world phenomena, and users should be aware of the trade-offs made between sufficient field data, computational expensiveness and model reliability (Nicholas, 2003; Hardy *et al*., 2003; Bates, 2004; Rodriguez *et al*., 2004). Compared to the hydrodynamic model, the morphodynamic models have even more sources of uncertainty (e.g. Pinto *et al*., 2006). They are also rather infrequently used today, and their functionality in natural environments has not been studied to a large extent. In this study, the functionality and sensitivity of hydro- and morphodynamic models in naturally meandering channels are assessed.

2.4 Fluvial geomorphology of meander bends

The planfom of a meandering river is characterised by bends and inflection reaches connecting the bends. A meander bend usually consists of a gentle point bar attached to the convex side and a deep pool by the steep concave side (Leopold and Wolman, 1960). A riffle is located at the inflection point. Many quantitative parameters characterising the meander planform have been implemented. Various definitions to the parameters can be found in the literature and care must be taken in deriving scientific facts based on the parameters (Hooke, 1984). Sinuosity stands for the ratio of the length of the river along the thalweg to the length of the valley (e.g. Friend and Sinha, 1993). Meander wavelength is the distance between the inflection points of successive bends on the same side of the river, and amplitude is the straight distance between the bend apices of successive bends perpendicular to the down valley axis (Leopold and Wolman, 1960) (Fig 2). The planform types can be classified into simple symmetric, simple asymmetric, compound symmetric and compound asymmetric (Brice, 1974) (Fig 3).

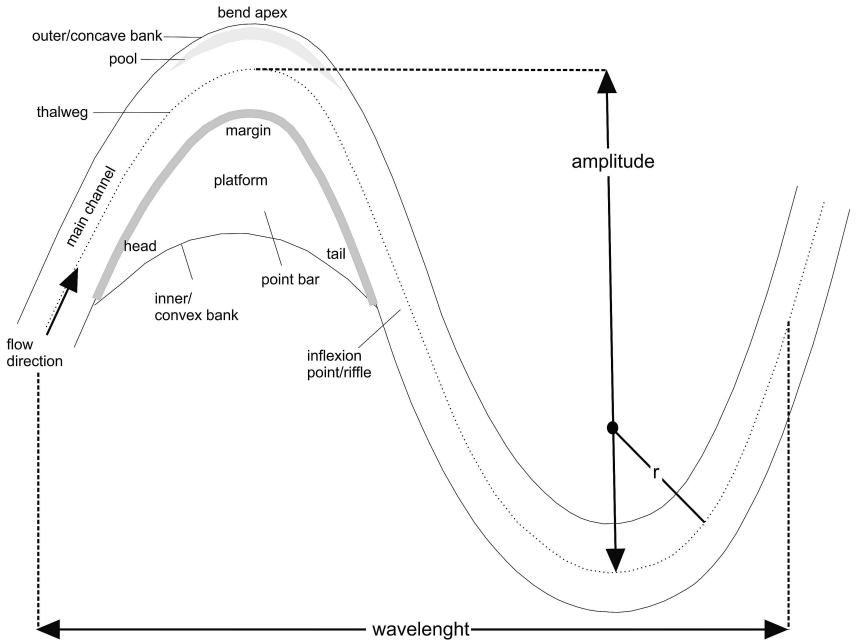

Fig 2. Terminology and parameters of a meander planform. The planform of the figure consists of two bends. Head, tail, platform and margin are parts of a point bar and are marked in the bend on the left. The r stands for radius of curvature.

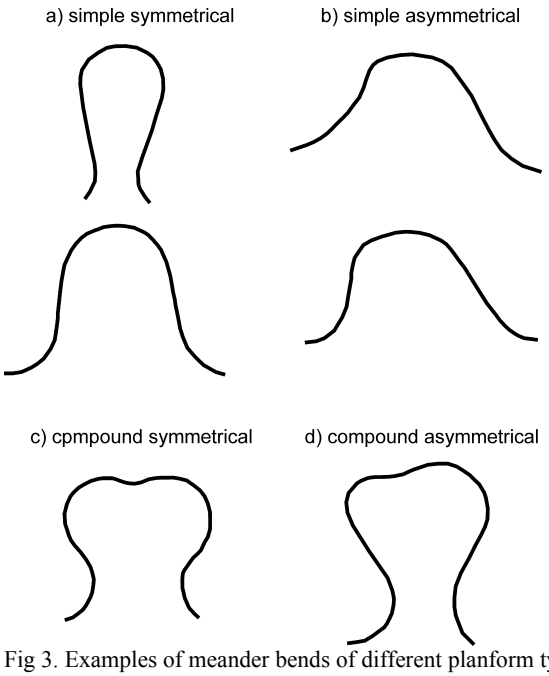

Fig 3. Examples of meander bends of different planform types after Brice (1974).

The curved shape of the channel and the transverse bed slope of the point bar induce a certain three-dimensional flow field, which in turn controls the sediment transport and

channel-bed morphology, maintaining the channel curvature and meander evolution (Hooke, 1975). When the flow enters a meander bend, the high velocity core (HVC) is situated near the inner bank, shifting gradually towards the outer bank along the bend due to the shoaling of the flow over the point bar and the bend curvature (Leopold and Wolman, 1960; Dietrich *et al*., 1979; Dietrich and Smith, 1983) (Fig 4). The outward flow causes a super elevation at the concave (outer) bank, which enforces a downwards flow along the outer bank, continuing as an inwards near-bed flow and upwards flow at the inner bank (e.g. Bathurst *et al*., 1979; Bridge and Jarvis, 1982; Dietrich and Smith, 1983; Termini and Piraino, 2011) (Fig 4). This circulating cell is called secondary circulation of flow (Fig 4). The outward flow may, however, dominate the entire water column at the upstream part of the point bar, limiting the secondary circulation to the pool and downstream part of the point bar (Dietrich and Smith, 1983). Further, at bends with a steep outer bank, a small cell of reverse rotation may appear near the outer bank (e.g. Bathurst *et al*., 1979; Thorne *et al*., 1985; Blanckaert and Graf, 2001). These flow structures cause the near bed flow velocities to be stronger downstream of the bend apex compared to the upstream part. This is called the submergence of the HVC (e.g. Rodriguez *et al*., 2004) (Fig 4). The strength of the secondary circulation has been noted to increase proportionally to the relative curvature and discharge (e.g. Engelund, 1974; Bathurst *et al*., 1979; Ferguson *et al*., 2003). With very high discharge, however, it has been noted to diminish or saturate (Bathurst *et al*., 1979). Other studies have shown that the secondary circulation may not form with a large width-to-depth ratio (Leopold and Wolman, 1960; Termini and Piraino, 2011) or in channels with very high curvature (Blancaert, 2009; Ottewanger, 2012).

The flow structures have major effects on the meander bend morphodynamics (Dietrich and Smith, 1984). Due to the transverse shift of the HVC towards the outer bank, the maximum stream power and sediment flux shifts from the inner bank towards the outer bank with distance downstream. The outwards flow throughout the water column at the upstream part of the bend and over the point bar head, combined with the gravitational force enforcing large particles towards the pool, intensifies the outwards-directed sediment transport (Dietrich and Smith, 1984). As the high velocities locate close to the concave bank at the bend exit, low flow velocities control the bar tail. This, accompanied with a recirculation zone that may be generated at the point bar margin beyond the apex, leads to deposition of fine material over the point bar platform (i.e. top) and tail (Bridge and Jarvis, 1976; Ferguson *et al*., 2003; Frothingham and Rhoads, 2003; Pyrce and Ashmore, 2005). Due to the inwards, near-bed flow and the recirculation, scroll bars may form on the point bar margin beyond the apex (Gautier *et al*., 2010; Kleinhans and van den Berg, 2011).

During very high discharges, the flow might straighten its way across the point bar platform as a chute current, eroding a chute channel at the inner bank with chute bars and a high concentration of coarse grain sizes over the point bar head and chute (e.g. McGowen and Garner, 1970; Bridge and Jarvis, 1976; Dietrich and Smith, 1984). With lower discharge, the HVC is located closer to the outer bank at the bend entrance and shifts towards the outer bank further upstream compared to high discharge (Hooke, 1975). Thereby, during low discharges, the current over the bar head also remains weak and diminishes, which enables filling of small particles further upstream on the point bar margin (McGowen and Garner, 1970; Pyrce and Ashmore, 2005).

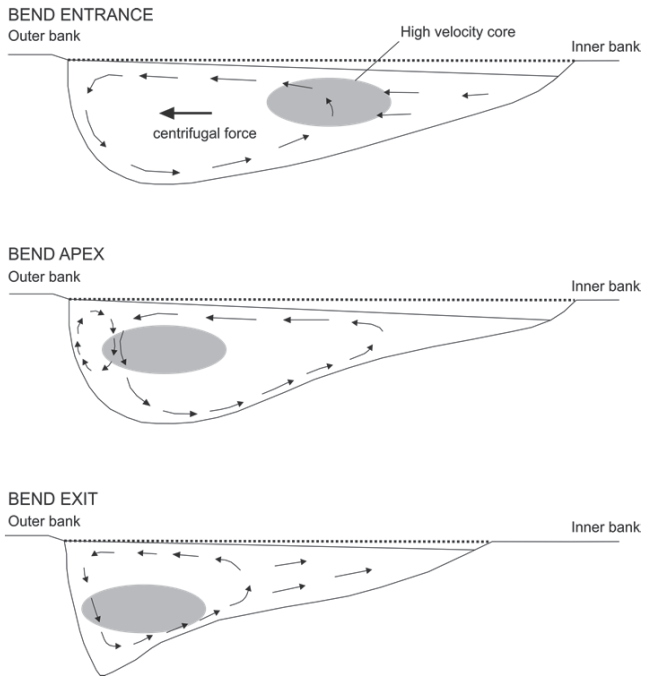

Fig 4. A simplified model of the flow structure over a meander bend. The three cross sections represent different parts of the bend: upstream, middle, and downstream. The grey ellipse represents the high velocity core and the arrows illustrate the direction of the secondary flow.

The 3-dimensional flow-sediment interactions maintain a continuous development of the meandering channel; many conceptual models describing the meander evolution have been produced (e.g. Brice, 1974; Hickin, 1974; Hooke, 1977). The erosion at the point bar head and convex bank beyond the apex and deposition over point bar tail are key factors of the meander evolution. They lead to a gradual increase in the meander amplitude, and the bend becomes sharp. The sinuosity increases, and the point bar grows laterally towards the outer bank (Brice, 1974; Hickin, 1974; Hooke, 1977; Blanckaert, 2011). Thus, the point bar of a mature meander bend experiences deposition mostly over the margins, and the emphasis of the deposition shifts from downstream to upstream of the apex (Pyrce and Ashmore, 2005). The outer bank erosion occurs further upstream, and the asymmetry of the bends increases, forming a compound bend and continuing to a cut-off, a sudden decrease in curvature (Hickin, 1974; Hooke, 1995). The bend deformation also has implications to the flow over the bend, as the bend curvature and point bar geometry effect on the secondary flow formation and location of the HVC (e.g. Ottewanger *et al*., 2012). It has been stated that the secondary flow strengthens as the curvature increases; however, in very sharp bends the secondary circulation is saturated and no further increase in secondary flow is expected (Blanckaert, 2009). This may inhibit the meander migration (Blankaert, 2011).

Even though general features exists in meandering rivers around the world, many recent studies have also indicated that individual characteristics of the bends and local factors of the streams may have a strong influence in the fluvio-morphological processes of the meander bends and on the evolution of the river (e.g. Hooke, 2007b; Gautier *et al*., 2010; Seminara, 2010; Hooke and Yorke, 2011; Kleinhans and van den Berg, 2011). In addition, the flow structures and thereby morphological changes of one bend depend on the bend upstream (Leopold and Wolman, 1960; Engelund, 1974; Dietrich and Smith, 1983). The deeper understanding of the mechanisms of meandering require detailed measurements of bed

geometry and its changes and flow characteristics over several bends (Hooke and Yorke, 2010). With the possibilities provided by the new measurement technologies and computational models, these individual processes may be investigated in detail and with higher spatial and temporal resolution than has been possible previously.

3 FLUVIO-GEOMORPHOLOGICAL BACKGROUND OF THE STUDY AREA

This study is performed on a sand-bed meandering river in Sub-Arctic Finland, where typically one significant flood event, the snow-melt induced spring flood, occurs annually in the rivers. The coldest temperatures in the region during the winter are from -45°C to -50°C, and the average annual temperature (1981-2010) is between -1°C and -2°C (Finnish Meteorological Institute, 2014) (Fig 5a). On average, the thermal winter (i.e. when the temperature is permanently below zero) starts in mid-October. The surface water of the rivers is frozen normally from October to May. The spring flood starts rising soon after the ice break up, which takes place during May. The vegetation of the area is dominated by low alpine birches and sprigs. The whole area is characterised by the moraine and formations generated by the retreat of the last continental ice ~10000 years ago.

The study is located in the meandering Pulmanki River, which is a tributary of the Tana River draining to the Arctic Ocean (Fig 5b). The Pulmanki River flows in the valley of Pulmanki, on the floor of which tens of metres of glacio-fluvial material has been deposited during the retreat of the continental ice (Mansikkaniemi and Mäki, 1990). Thus, the sediment availability is guaranteed, which is often the case in the proglacial river valleys (e.g. Ferguson and Ashworth, 1986; Warburton, 1990). The Pulmanki River has eroded a 30 m deep and 20–50 m wide channel into the sediments, on which it evolves actively; oxbow lakes and recent neck-cut-offs have been reported (Mansikkaniemi and Mäki, 1990). The river is divided into two parts by Lake Pulmanki, and the study reach is located upstream of the lake (Fig 5b). The total catchment area of the Tana River is 5095 km², and the sub-catchment area of Pulmanki River upstream of Lake Pulmanki is about 480 km² (Fig 5a). The highest point of the catchment is 443 m.

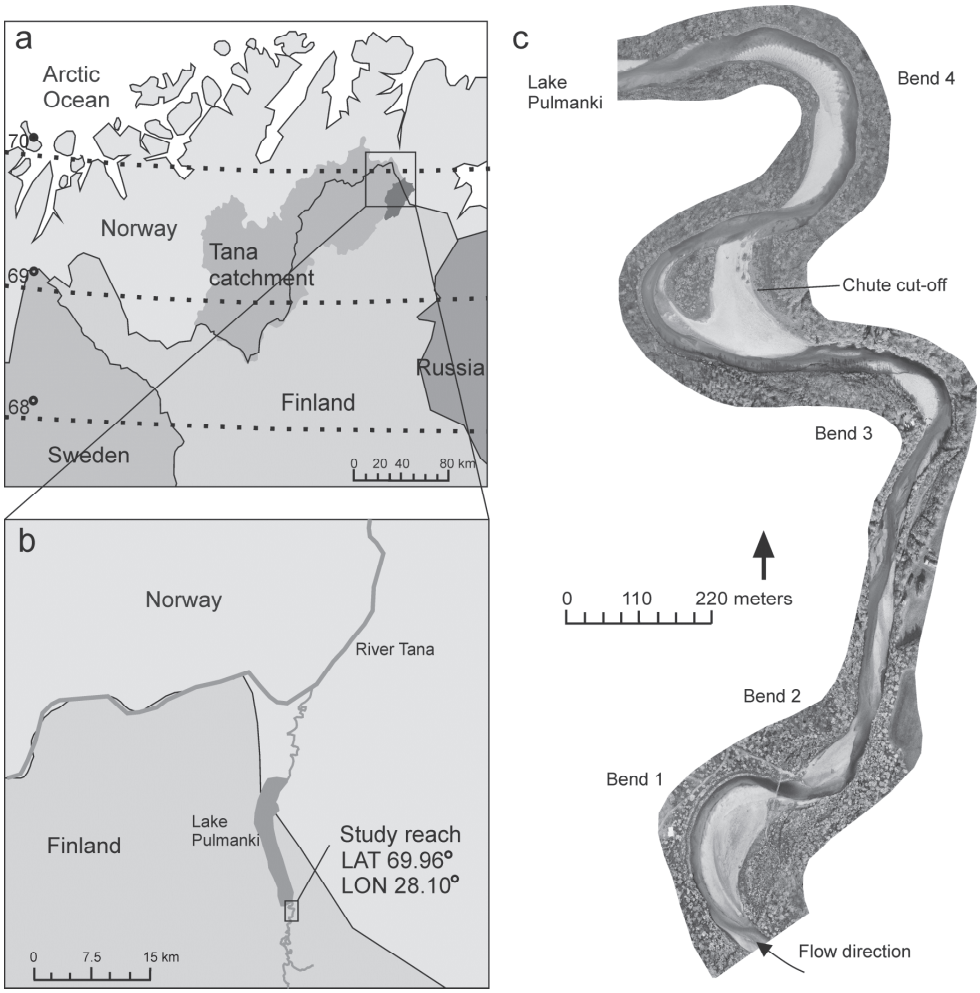

Fig 5. a) The study site is located in the sub-arctic Finland, close to the border of Finland and Norway. The catchment of Pulmanki upstream of Lake Pulmanki is marked in the figure in dark grey. It is a part of the Tana catchment. b) The study area at Pulmanki River is located upstream from Lake Pulmanki. Downstream of the lake, Pulmanki River converges into Tana River. c) The study reach and the studied bends. The aerial photograph was taken in 2013 during low water stage. The second bend downstream is not examined in this study. During the high water stage, a chute cut-off develops through the bend. The cut-off is unvegetated.

The study reach is 2.5 km long (along the thalweg) and is restricted to Lake Pulmanki on the downstream side (Fig 5c). The slope of the reach is ~0.02%. It consists of five meander bends, four of which are examined in this study (Table 1, Fig 6). The water level of Lake Pulmanki is ~13.4 m above sea level, and the water surface elevation during the low water stage upstream of Bend 1 is ~15.8 m. The discharges vary between 1.5 and 70 $m^3 s^{-1}$. The typical spring flood peak discharge is 40–55 $m^3 s^{-1}$ during May. By the middle of June, the discharge normally decreases to 2–8 $m^3 s^{-1}$, remaining low for the rest of the unfrozen period.

Table 1. The quantitative characteristics of the four bends examined in this study and the numbers of the papers in which a certain bend has been studied. Even though a certain bend might have been a part of the modelled area in a paper, if it is not investigated, it is not considered a part of that paper. The locations of the bends are marked in Fig 5. The width and radius of curvature are the values at the bend apex. The planform types are A=simple symmetric, B=simple asymmetric, C=compound symmetric, D= compound asymmetric

	Bend 1	Bend 2	Bend 3	Bend 4
Sinuosity	1.6	1.2	1.4	1.8
r. of curvature	120 m	47 m	110 m	155 m
Width (low flow)	15 m	17 m	17 m	20
Width (bankfull)	100 m	65 m	60 m	79 m
Point bar size	14390 m^2	3520 m^2	3800 m^2	16100 m^2
Paper	IV	IV	I, II, III, IV	I
Planform type	B	A	A	D
Erosion protection	Yes	No	No	Yes

The meander point bars of the studied bends are normally inundated only during the spring flood (Fig 6). The concave banks are steep and highly sensitive to erosion. The river is unregulated but some of the bends on the study reach have a man-made erosion protection along the concave bank due to the high rate of bank erosion (Table 1). The stream bed is not vegetated. The bed and bank material is mostly sand. Steep concave banks consist of the smallest grains ($D_{50} < 0.5$ mm). On point bars and in the main channel the D_{50} of the bed material can vary between 0.2-3 mm. Around the thalweg, grains up to few centimetres can be found. The bed material is mostly poorly sorted.

Sandy bed load (transport rate ~1 x 10^{-4} m^3 s^{-1}) dominates the sediment transport of the study area during both high and low discharges. The highest suspended load concentration takes place during the rising flood stage (180–280 mg/l). During the low summer flow, the suspended load is minimal. Thus, as the discharge decreases, the percentage of bed load out of the total load increases. Increased run-off from the surrounding areas may have a notable effect on the suspended load transport also during the low discharge. Flood events induce notable changes in the channel and point bars: vertical changes of +/- 0.5 metres are normal on the point bar areas

The Pulmanki River was selected for a study area because it experiences notable and predictable flooding annually, and the channel is dynamic with meandering planform and migration and its bends are in different phases of development. The characteristics of the study area are comparable to many other study reaches on which studies over small spatial and temporal scale have been realized (see Table 1 in Paper III). However, the effects of the ice cover to the revers hydro- and morphodynamics has not been dissected in this study and the research concerning to it is limited in general (cf. Ettema, 2002). The ice cover and the associated intensive flood events are, though, typical to Arctic and sub-Arctic rivers. Pulmanki River is also reasonably small which enables detailed measurements. Pulmanki Thereby, Pulmanki River provides an ideal natural laboratory to study the fluvio-geomorphological processes of a meandering river in natural environment.

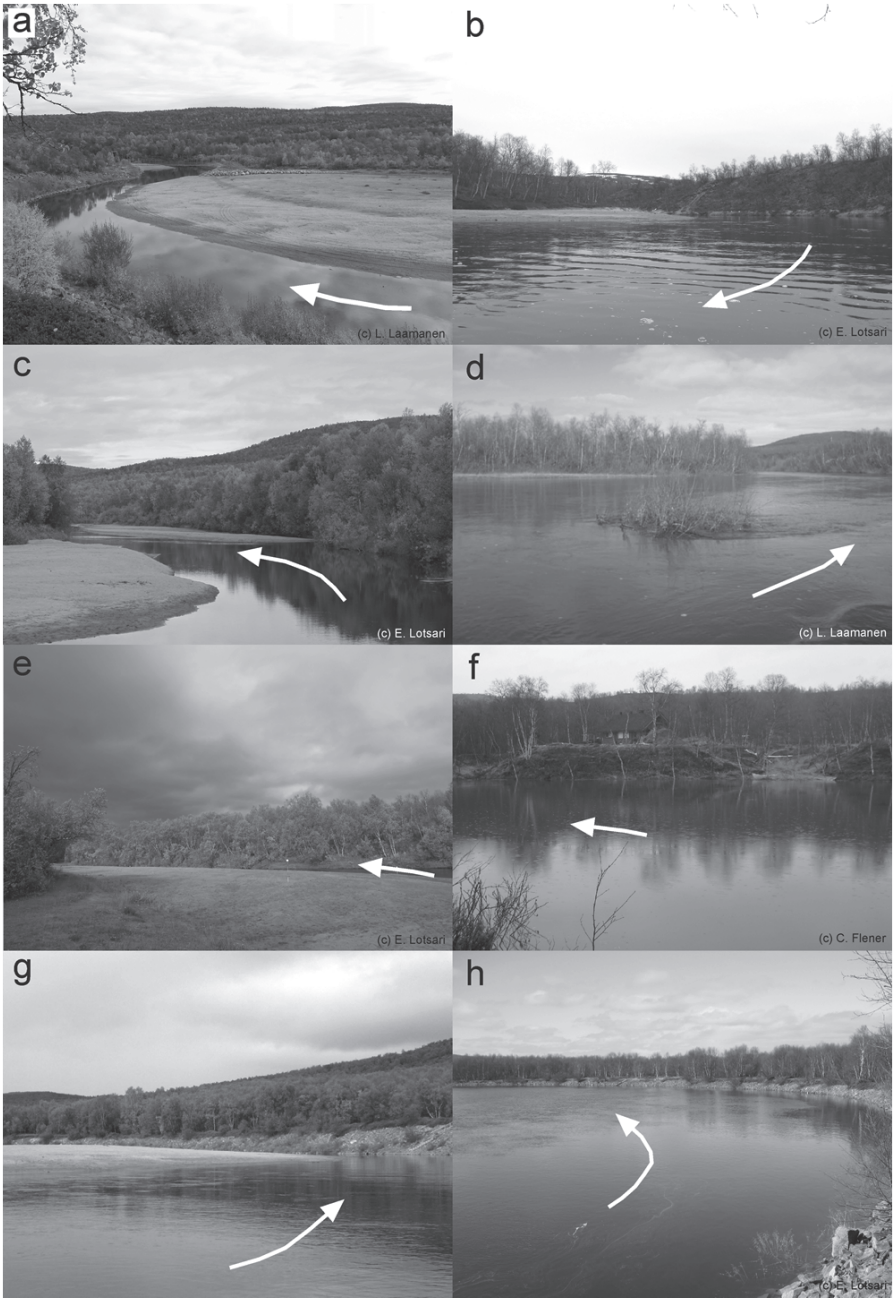

Fig 6. The four studied bends during high (left) and low (right) water stage. a-b) Bend 1 c-d) Bend 2 e-f) Bend 3 g-h) Bend 4

4 METHODS

In this thesis, sophisticated close-range remote sensing methods (ADCP, MLS, TLS, UAV) were exploited in parallel with conventional field measurements in order to explain and quantify the processes in meander bends with increased reliability and detail. In addition, the spatial and temporal resolution of the data was enhanced using hydro- and morphodynamic models. The methods used in each paper are presented in Table 2.

Table 2. The data and approaches exploited in the four papers of this thesis, and the methods used to collect the data

	Paper I	Paper II	Paper III	paper IV
Flow discharge (ADCP)	x	x	x	x
Flow velocity (ADCP)		x	x	x
3D flow velocity (ADCP)	x	x		
Water level changes (level loggers + RTK-GPS)	x	x	x	x
GSD (dry-sieved sediment samples)	x	x	x	x
Bed load (Helley-Smith sampler)		x		x
Suspended load (depth-integrated water sampler)		x		x
DTM (TLS + MLS)	x	x	x	x
DoD (TLS + MLS)	x	x	x	x
Bathymetric model (Standard echo sounder)			x	
Bathymetric model (Side scanning sonar)		x		
Bathymetric model (remote controlled ADCP)				x
2D hydrodynamic model (TUFLOW, Delft3D)		x	x	x
3D hydrodynamic model (Delft3D)		x		
Morphodynamic model in 2D and 3D (Delft 3D)		x		
Sediment transport model in 2D (Delft3D)				x
High-resolution aerial photograph (UAV)				x
Field observations of fluvial formations (located with RTK-GPS)				x

4.1 Close-range remote sensing and field data collection and processing

4.1.1 Flow characteristics

As the study reaches of each paper are slightly different, the locations of the flow measurements also vary between the papers. However, the same principles were used in each study. The flow characteristics measured include water level, discharge and flow velocities in 3D. The measurements were carried out between 2009 and 2013. The variation of the water level was derived based on water pressure sensors (Solinist Levelogger Gold, Model 3001),

which measure the changes in the height of the water column above the sensor based on water and air pressure. The depth sensors were installed into the river bed immediately after the ice break up, and the logging interval was set to 15 minutes. The air pressure was measured near the study area with the same recording interval to compensate for the water pressure sensor measurements. The water depth was recorded throughout the unfrozen period. The water level sensors were located in the upstream and downstream boundaries and in the middle of the study reach depending on the year and study. In paper I, only the water level recorded at the upstream boundary was used. In all other papers (II, III and IV), three water level records were exploited in building and calibrating computational models. The water depth measurements were tied to a geographical coordinate system using RTK-GPS measurements from various discharge magnitudes.

Discharge measurements were carried out using ADCP at the upstream boundaries of the study reaches. Another criterion when choosing the discharge measurement location was that the river reach should be as straight as possible. The sensor used in this study was RiverSurveyor M9, which has four 3 MHz and four 1 MHz transducers and a vertical beam. Discharge was the measured by transferring the device slowly across the river. At least four discharge measurements, which all fell within 5% of each others, were required before accepting the result. Discharge rating curves were then built using a regression model, which converges the discharge measurements with the continuous water level record of the same location. The discharge rating curve of the upstream boundary of the study reach was used in each paper of this study.

The ADCP device was also used to measure the flow velocities along river cross-sections in three dimensions. The locations of the transects were chosen visually to represent the radius of curvature of the bend in that location. The device was equipped with a differential global positioning system (DGPS) to link the flow measurements to a geographical coordinate system. The depth-averaged flow velocity measurements were used to calibrate and validate computational models (papers II, III and IV). The 3D cross-sectional flow fields were used to analyse the fluvio-morphological processes over meander point bars (paper I) and to assess the 3D computational reconstruction of the flow field in a meander bend (paper II).

4.1.2 Sedimentological data

Conventional methods were used in deriving the information related to sediment size and transport. Grain sizes of the sediments on the river bed and point bars were defined based on sediment samples (papers I, II, III and IV). The samples of approximately 0.5 kg were taken from the river bed and point bar surfaces after each flood event. A van Veen type of sampler was used to take a sample from inundated locations. The locations of the samples were measured using RTK-GPS. The locations of the samples varied between the studies according to the focus of the study. All of the sediment samples were dry sieved with a sieve interval of half phi.

The grain size data were used to analyse the morphological changes over the point bars (papers I, III, and IV) and as input data in morphological models (papers II and IV). In the case of a morphological model, the sampling was realised over the modelled area, and the D50 values of the samples were interpolated to cover the whole area.

Sediment transport was measured during high and low discharge using a hand-held HelleySmith-sampler on one river cross-section in the middle of the study reach (papers II and IV). The Helley-Smith-sampler was chosen, because it is cost efficient and has been proven to provide relatively reliable estimates of the actual bed load transport (e.g. Hubbel *et al*., 1981). It is also one of the most used devices to measure the bed load in sand-bed rivers

(e.g. Rennie *et al*., 2002; Hicks and Gomez, 2003; Rathburn *et al*., 2013). The sampler used had a 152 x 152 mm opening and 3.22 expansion ratio and the polyester mesh bag with 0.02 mm mesh. The measurements were taken at three verticals along the cross-section. To ensure the representativeness of the samples, three samples of three-minute durations were taken from each vertical. Thus, in total nine samples were taken to measure the total bed load through the cross-section. The average value of the dry mass of the three samples of each vertical was then calculated and the bed-load transport rate through the cross-section was composed by dividing the resultant average value with the product of the width of the intake opening and sampling period. The measurement campaign was repeated a few times during different discharge circumstances (high, medium and low) depending on the year. Sampling efficiency of 1.5 was assumed (Glysson, 1993). The divergence of the measured bed load of the same vertical during one measurement campaign remained below 20 %.

The temporal variation of the sediment input from the upstream parts of the river to the study reach is notable due to, for example, the slumping and mass failures of the high river banks over the bends. Also the measured bed load transport of this study showed notable temporal variation and no connection between bed load transport rate and discharge or flow velocity was observed. Large spatial and temporal variations in bed load transport are common according to other studies as well due to, for example, bedforms migrating past the sampling points (e.g. Gomez *et al*., 1990; Rennie *et al*., 2002). Concurrently with the bed load measurements, depth-integrated water samples, based on which the suspended load was defined, were taken from each of the three verticals. The sediment transport rates were used to calibrate the morphological models in papers II and IV.

4.1.3 Topographical survey (LiDAR-based approaches)

The topographical data in this study were based on close-range remote sensing methods. In each paper of this study, one flood event (varying between the papers) and its effects on the particular study reach is examined. Therefore, the topographical survey campaigns always consist of the collection of pre- and post-flood data. The topographical data were collected using TLS and MLS (papers I, II, III and IV). The laser scanning campaigns were conducted during the low water stage, because infra-red LiDAR, which was used in this study, requires a dry scanning target. Thus, the pre-flood topographical data were collected before the winter, when the exposed area was largest. The terrain areas were assumed to remain unchanged under the snow cover during the winter.

TLS was used to collect detailed topographical data over the meander point bars and to provide reference data for MLS data verification and accuracy (Table 3, Fig 7a). The locations of the scan stations and sphere targets were positioned using the RTK-GPS. The scans were transformed to global coordinates (WGS84) based on the measured locations of the scanner and the sphere targets: the sphere targets were detected from the laser data of each scan, and the centre point of the target was defined based on the points reflected from the target. Noisy points (i.e. points below and above ground surface) were removed from the TLS data. An absolute accuracy on ~0.01 m was achieved for the point clouds (point density of ~3000 points/m^2.)

Table 3. The applied TLS scanners in papers I-IV. The year of the measurement campaign is marked in the first row.

	2008	2009	2010	2012	2013
Scanner	LeicaHDS6000	LeicaHDS6000	Leica HDS6100	FAROFocus3D	FAROFocus3D
Scanner type	Phase-based	Phase-based	Phase-based	Phase-based	Phase-based
Papers	I, III	I, II, III	II	IV	IV

In order to enhance the topographical data collection, three different MLS setups were used in this study (Table 4, Fig 7 b-d). A boat-based mobile mapping system (BoMMS) was exploited in papers I, III and IV (Fig 7b). A cart-based mobile mapping system (CartMMS) was used in papers I and III (Fig 7c). In paper IV, a backpack-based MLS setup (Akhka) was used (Fig 7d). All of the MLS systems include a temporally synchronised TLS and a navigation system, which includes a GPS receiver and an IMU. The details of each measurement campaign are presented in Table 4. The BoMMS was used to enhance the data collection over the river banks, which are not easily achievable or measurable using TLS. The two other MLS setups, i.e. the cart- and backpack-based, were used to improve the spatial coverage of the BoMMS and TLS.

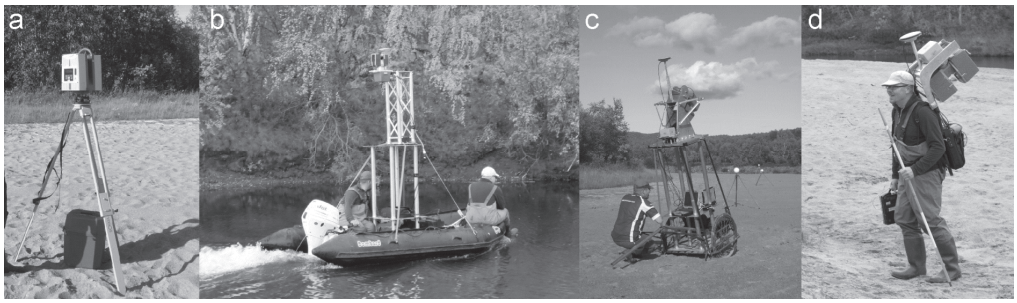

Fig 7. The LiDAR setups applied in the study. Further details of the scans and setups are collected in Tables 2 and 3. a) Terrestrial laser scanner b) Boat-based mobile mapping system (BoMMS) c) Cart-based mobile mapping system (CartMMS) d) Backpack-based mobile mapping system (Akhka)

Table 4. Details of the MLS campaigns realised in this study. The types of the MLS platforms ('mobile system') are numbered as follows: 1= BoMMS, 2= CartMMS, 3= Akhka

	2008	2009	2010	2012	2013
Scanner	FAROLS880HE80	FAROPhoton80	FAROPhoton120	FAROPhoton120	FAROFocus3D120
RMSE	0.029-0.046	0.04-0.051	0.015	0.013-0.015	0.014-0.018
Scanning freq.	15 Hz	30 Hz	49 Hz	49 Hz	60 Hz
Meas. freq.	120 kHz	120 kHz	244 kHz	488 kHz	488 kHz
Mobile system	1	2	3	1, 3	1, 3
Paper	I, III	I, II, III	II, III	IV	IV

The trajectory of the MLS sensor was calculated afterwards by integrating the observations of the GPS (1Hz) and IMU (100Hz). The point clouds were geo-referenced to the geographic coordinate system (WGS84), and the ground points were classified using the method based on the work of Axelsson (2000) using TerraScan software. The method is based on a progressive TIN densification. The program classifies the lowest local points as the initial ground points from a large area (e.g. using an 80m x 80m grid) and creates an initial TIN. New laser points are then added to the model iteratively based on assigned criteria. Competitive results have been gained with in-ground filtering tests (Sithole and Vosselman, 2004; Meng *et al*., 2010). The accuracy of the resultant terrain model was defined by comparing the MLS point cloud to the TLS data on the overlapping areas. In the process, GPS- and IMU-based systematic errors were also corrected. The vertical Root Mean Square Errors (RMSEs) of the DTMs of each year are presented in Table 4.

DTMs of certain point spacing (0.1-0.25 m depending on the study) were then created based on the ground point clouds by calculating the average elevation value of the points falling inside a grid cell. The resultant regular grids were used in change detections over the point bars (papers I, II, III and IV) and to build the initial geometry for computational models (papers II, III and IV). The change detection was based on a DTM of difference (DoD), which is a product of subtraction of pre- and post-flood DTMs.

4.1.4 Bathymetric survey (Echo sounding)

The bathymetric data were also collected using close-range remote sensing. The bathymetric data were needed to create the initial geometries for the computational models (papers II, III and IV). Three kinds of echo sounders were exploited. In paper II, the bathymetric data was based on a side-scanning echo sounder (Aquatic Sonar's Swathe Surveyor) consisting of two side-looking and one down-looking transducers. A point spacing of 0.25 m was achieved. In paper III, a separate echo sounder with one beam attached on an inflatable boat and equipped with RTK-GPS was used. A point spacing of approximately 2 m was achieved. In paper IV, the bathymetric data were collected with a 0.5 MHz echo sounder integrated to an ADCP device (Son-Tek RiverSurveyor M9). The ADCP device was attached to a remote-controlled boat and equipped with an RTK-GPS (Fig 8a). The remote-controlled boat enabled bathymetric surveys on shallower areas compared to a normal boat without disturbing the river bed; its draught is only 0.17 m (Fig 8b). In that case, a point spacing of 1-2 metres was achieved.

The bathymetric surveys were realised immediately after the ice break up, during the rising flood stage. Thus, the initial geometries of the computational models consisted of topographical data collected before the winter and bathymetric data collected after the winter. The initial geometries for the computational models were built by combining the topographic and bathymetric point clouds, after which a seamless digital elevation model (DEM) of the whole modelled area was created.

The post-flood bathymetric data were not collected due to the extremely low water depths of the area. Thus, the change detections were realised only over the exposed areas.

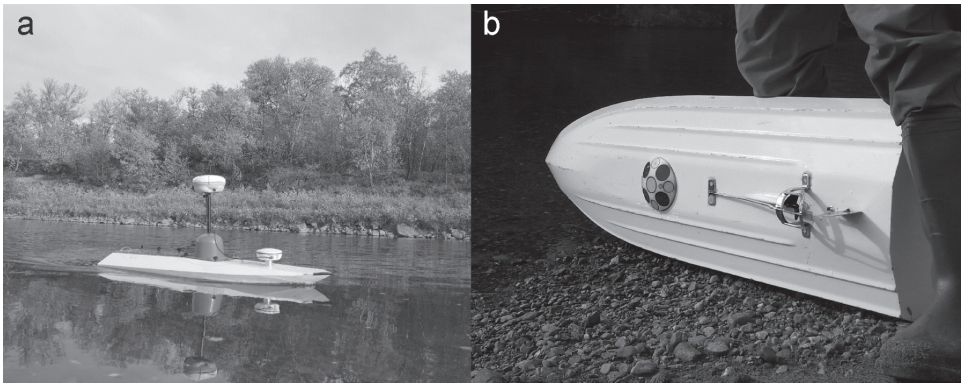

Fig 8. The ADCP device attached to a remote-controlled boat and equipped with RTK-GPS. a) In action b) From below.

4.1.5 UAV-based aerial photographs

In paper IV, aerial photo mosaic collected from an unmanned aerial vehicle (UAV) was exploited in morphological interpretation of the flood-based formations on the point bars (Fig 9a-b). The photographs were taken from a Droidworx Skyjib 8 octacopter with a Samsung NX300 micro-DSLR camera. The average flying altitude was 84 metres, and the photographs were positioned using RTK-GPS. In total, 1223 images were used in creating the photomosaic of the whole study area. The final resolution of the photomosaic was 5 cm. Some field observations, located with RTK-GPS, were realised in order to assist the interpretation of the photograph.

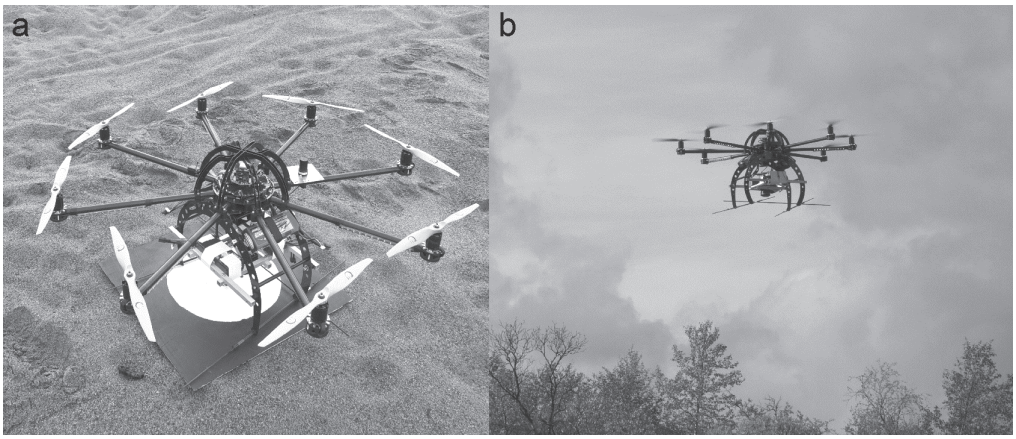

Fig 9. Unmanned aerial vehicle equipped with Samsung NX300 camera and RTK-GPS collecting an aerial photo mosaic. a) Departing b) In action

4.2 Hydro- and morphodynamic modelling approaches

In this study, both 2- and quasi-3-dimensional CFD were used. Each simulation was performed over one spring flood event. The discharge rating curve was used as the upstream and water level variation as downstream boundary condition in each simulation. The hydrodynamic models (TUFLOW and Delft3D) were calibrated to match the water level

recorded from the middle of the modelled reach and flow velocity measurements. The calibration was realised by adjusting the roughness parameters and eddy viscosity. The modelled sediment transport rates (Delft3D) were adjusted to correspond with field measurements of bed load and suspended load transport. The transport magnitudes were calibrated by adjusting user-defined factors in sediment transport formulae.

4.2.1 2D and 3D hydro- and morphodynamic modelling of paper II

In paper II, the 2D and quasi-3D models with sediment transport and morphological change were run over the spring flood event of 2010 using the Delft3D-model. In the quasi-3D approach, the reduced vertical momentum equations read:

$$\frac{\partial P_h}{\partial \sigma} = -\rho g h \qquad \text{Equation 4}$$

P_h = hydrostatic pressure
σ = vertical sigma coordinate

and the horizontal momentum equations in x- (equation 5) and y- (equation 6) directions are written as follows:

$$\frac{\partial u}{\partial t} + u\frac{\partial u}{\partial x} + v\frac{\partial u}{\partial y} + \frac{\omega}{d}\frac{\partial u}{\partial \sigma}$$

$$= -\frac{1}{\rho_0}P_x + \frac{1}{d^2}\frac{\partial}{\partial \sigma}\left(V_v\frac{\partial u}{\partial \sigma}\right) + V_h\left(\frac{\partial^2 u}{\partial x^2} + \frac{\partial^2 u}{\partial y^2}\right) \qquad \text{Equation 5}$$

$$\frac{\partial v}{\partial t} + u\frac{\partial v}{\partial x} + v\frac{\partial v}{\partial y} + \frac{\omega}{d}\frac{\partial v}{\partial \sigma}$$

$$= -\frac{1}{\rho_0}P_y + \frac{1}{d^2}\frac{\partial}{\partial \sigma}\left(V_v\frac{\partial v}{\partial \sigma}\right) + V_h\left(\frac{\partial^2 v}{\partial x^2} + \frac{\partial^2 v}{\partial y^2}\right) \qquad \text{Equation 6}$$

where:

u and v= velocity components in Cartesian coordinate system (m s^{-1})
g = gravitational acceleration (m s^{-2})
$P_{x,y}$ = pressure (Pa)
d = water depth (m)
ρ_0 = reference density of water (kg m^{-3})
ω = vertical velocity component in σ-coordinate system (m s^{-1})
V_v = vertical eddy viscosity (computed by k-e)
V_h = horizontal eddy viscosity (user defined)

In a depth-averaged (2D) approach, the horizontal momentum equations are written as follows:

$$\frac{\partial u}{\partial t} + u\frac{\partial u}{\partial x} + v\frac{\partial u}{\partial y} + g\frac{\partial h}{\partial x} + \frac{gu\sqrt{u^2+v^2}}{C^2 h}$$

$$= -\frac{1}{\rho_0}P_x + F_{sec,x} + V_h\left(\frac{\partial^2 u}{\partial x^2} + \frac{\partial^2 u}{\partial y^2}\right) \qquad \text{Equation 7}$$

$$\frac{\partial v}{\partial t} + u\frac{\partial v}{\partial x} + v\frac{\partial v}{\partial y} + g\frac{\partial h}{\partial y} + \frac{gv\sqrt{u^2+v^2}}{C^2 h} = -\frac{1}{\rho_0}P_y + F_{sec,y} + V_h\left(\frac{\partial^2 v}{\partial x^2} + \frac{\partial^2 v}{\partial y^2}\right)$$ Equation 8

The F_{sec} represent the correction terms of the effect of secondary flow correction, which accounts for the horizontal effective shear-stresses originating from the secondary flow (Delft3D-FLOW, 2011, p. 236 onwards). The pressure gradients are calculated as follows (assuming a constant density of water):

$$\frac{P_x}{\rho_0} = g\frac{\partial h}{\partial x} + \frac{\partial p}{\rho_0 \partial x}$$ Equation 9

$$\frac{P_y}{\rho_0} = g\frac{\partial h}{\partial y} + \frac{\partial p}{\rho_0 \partial y}$$ Equation 10

where:

p = atmospheric pressure (Pa)
h = water level (m)
C = Chezy's coefficient ($m^{0.5} s^{-1}$)

The final terms of the horizontal momentum equations (eq.5-8) represent the simplified horizontal Reynolds stresses. The horizontal continuity equation (conservation of mass) for 2D and 3D applications is written as follows:

$$\frac{\partial \zeta}{\partial t} + \frac{\partial [h\bar{u}]}{\partial x} + \frac{\partial [h\bar{v}]}{\partial y} = 0$$ Equation 11

where:

ζ = water surface elevation (m)
$\bar{u} and \bar{v}$ = depth-averaged velocity components (ms^{-1})

The vertical velocity in 3D approach is computed assuming hydrostatic pressure distribution using the following continuity equation:

$$\frac{\partial W}{\partial \sigma} = -\frac{\partial \zeta}{\partial t} - \frac{\partial [hu]}{\partial x} - \frac{\partial [hv]}{\partial y}$$ Equation 12

where W is the vertical velocity (in $m\ s^{-1}$).

The hydrodynamic model was calibrated by adjusting the roughness parameters and the horizontal eddy viscosity and diffusivity so that the modelled water surface elevation and flow velocity matched the measured ones. In Delft3D, the sub-grid scale mixing coefficients (horizontal and vertical viscosity and diffusivity) are approached as if they consisted of three parts: 2D turbulence, 3D turbulence and kinematic viscosity (Delft3D-FLOW, 2011, p. 199), 2D turbulence means the horizontal mixing and 3D turbulence means the vertical mixing. In the 2D simulation, constant eddy viscosity and diffusivity coefficients were used to maintain

model stability. They stand for the combined effect of 2D and 3D turbulences and the kinematic viscosity. In a 3D approach, a value of 1.4 $E^{-06}m^2$ s^{-1} was used for the kinematic viscosity, constant values were used for the 2D turbulence and the k-ε-turbulence closure model was used to determine the 3D turbulence (Delft3D-FLOW, 2011, p. 231).

The models' sensitivity to various user-defined parameters (grain size, roughness, transverse bed slope effect, sediment transport formula and secondary flow correction) was tested, and the results were compared and assessed relative to field measurements. Both Manning's and Chezy's roughness parametrisations were applied. The transverse bed slope effect was modelled using the following equation:

$$S_{b,x} = \left|S_b^{`}\right| \alpha_{bn} \frac{u_{cr}}{|\overrightarrow{u_b}|} \frac{\partial z_b}{\partial n} \qquad \text{Equation 13}$$

$\left|S_b^{`}\right|$ = magnitude of the unadjusted bed load transport
α_{bn} = user-defined coefficient (default is 1.5, values 0, 1.5 and 3 were tested in paper II)
u_{cr} = critical (near-bed) velocity
$|\overrightarrow{u_b}|$ = (near-bed) fluid velocity vector
$\frac{\partial z_b}{\partial n}$ = bed slope (normal to the unadjusted bed slope transport vector)

The effect of the secondary flow on the bed load transport direction in the 2D model was calculated as follows:

$$\tan(\gamma_\tau) = \frac{v - \alpha_I \frac{u}{U} I_s}{u - \alpha_I \frac{v}{U} I_s} \qquad \text{Equation 14}$$

in which

$$\alpha_I = \frac{2}{\kappa^2}\left(1 - \frac{1}{2}\frac{\sqrt{g}}{\kappa C}\right) \qquad \text{Equation 15}$$

where

I_s = spiral flow intensity (m s^{-2})
γ = angle between downstream and sediment transport direction
κ = Von Kármán constant
U = depth-averaged velocity

and the depth-averaged models' sensitivity to the secondary flow correction was tested by ignoring the secondary flow correction. The transport formulas of Engelund and Hansen (1967) and van Rijn (1993) were tested. In the Engelund & Hansen approach, the total sediment load is calculated as follows:

$$S_b = \frac{0.05\,\beta q^5}{\sqrt{g} C^3 \Delta^2 D_{50}} \qquad \text{Equation 16}$$

where:

Δ = relative density of sediment under water
β = calibration parameter (default=1)

In the van Rijn approach, so-called sink and source terms are used to calculate the sediment transfer between the bed and the flow. The terms appear near the river bed, above the van Rijn reference height (van Rijn, 1993). Bed-load transport occur below and suspended-load transport above the reference height, and the concentration of sediment in the reference layer is calculated as using the following formula:

$$c_a = f_{sus} 0.015 \rho_s \frac{D_{50} T^{1.5}}{a D_*^{0.3}}$$ Equation 17

where:

f_{sus} = calibration parameter
c_a = sediment concentration at reference height (kg m^{-3})
ρ_s = density of sediment particles (kg m^{-3})
D_{50} = median sediment diameter (m)
T = dimensionless bed shear stress

The quantities of the source and sink terms for the reference layer are calculated as follows:

$$Source = \frac{D_v c_a}{\Delta z}$$ Equation 18

$$Sink = c_{rl} \left(\frac{D_v}{\Delta z} + w_s \right)$$ Equation 19

where:

D_v = vertical eddy diffusivity (m^2 s^{-1})
c_{rl} = mass concentration of sediment in the reference layer (kg m^{-3})
Δz = vertical distance of the reference layer from the reference height a (m)

The suspended sediment transport is calculated by solving the 3D advection–diffusion equation:

$$\frac{\partial c}{\partial t} + \frac{\partial uc}{\partial x} + \frac{\partial vc}{\partial y} + \frac{\partial (W - W_s)}{\partial x}$$

$$= \frac{\partial}{\partial x}\left(D_x \frac{\partial c}{\partial x} \right) + \frac{\partial}{\partial y}\left(D_y \frac{\partial c}{\partial y} \right) + \frac{\partial}{\partial z}\left(D_z \frac{\partial c}{\partial z} \right) + S$$ Equation 20

where:

W_s = sediment settling velocity (m s^{-1})
c = sediment concentration (kg m^{-3})
D = eddy diffusivity (m^2 s^{-1})
S = source/sink term describing the erosion and deposition fluxes (kg m^{-2})

In a depth-averaged approach, the 4th and 7th terms of the equation 20, which represent the vertical gradients, disappear. Different equations are given to different sizes of sediment in suspension to calculate the fall velocity:

$$w_s = \begin{cases} \frac{(s-1)gD_s^2}{18V_k} & 65\ \mu m < D_s \leq 100\ \mu m \\ \frac{10V_k}{D_s}\left(\sqrt{1+\frac{0.01(s-1)gD_s^3}{{V_k}^2}}\right) & 100\ \mu m < D_s \leq 1000\ \mu m \\ 1.1\sqrt{s-1)gD_s} & 1000\ \mu m < D_s \end{cases}$$ Equation 21

where:

s = relative density of sediment (kg m^{-3})
D_s = diameter of sediment in suspension (m)
V_k = kinematic viscosity coefficient of water (m^2 s^{-1})

The magnitude (Equation 22, kg $m^{-1}s^{-1}$) and direction (Equations 23 and 24) of bed-load transport are computed as follows:

$$|S_b| = f_{bed} 0.5 n \rho_s d_{50} u_*^{'} D_*^{-0.3} T$$ Equation 22

$$S_{b,x}^{''} = \frac{u_b}{|q_b|}\left|s_b^{''}\right|$$ Equation 23

$$S_{b,y}^{''} = \frac{v_b}{|q_b|}\left|s_b^{''}\right|$$ Equation 24

where:

f_{bed} = calibration parameter
n = availability of sediment
u` = effective bed shear velocity (based on the velocity in the bottom layer)
D_* = dimensionless particle diameter
T = dimensionless bed shear stress
u_b,v_b = (near-bed) flow velocity components (depth-averaged in 2D approach) (m s^{-1})
q = (near-bed) flow velocity (depth-averaged in 2D approach) (m s^{-1})

First, the sediment transport rates of both approaches, Engelund & Hnasen and van Rijn, were calibrated to match the field measurements by adjusting the parameter β in equation 16 for the Engelund and Hansen formula and parameters f_{sus} and f_{bed} in equations 17 and 22, respectively, for the van Rijn formula.

The grain size distribution over the area evolves as the flow transports the sediment. The initial grain size distribution was based on 210 sediment samples over the reach. The model was implemented over a curvilinear, unstructured grid, with the cell size varying between 0.5 and 2 m^2. The 3D model contained eight vertical layers. The bed shear stress (N m^{-2}) distribution over a cross-section at a bend apex was extracted at three flow stages from both 2D and 3D implementations. In Delft 3D, the bed shear stress is calculated using the following formula:

$$\tau = \frac{g\rho_0 u|u|}{C^2}$$ Equation 25

In the 3D approach, the flow velocity is the horizontal near-bed velocity, and in the 2D simulation, the near-bed velocity is determined from the depth-averaged velocity, assuming a

logarithmic velocity profile. As the model was run in water of temperature lower than 10°C, the BSS values were converted to represent the BSS in a water temperature of +5 °C by multiplying the values by the following formula:

$$\left(\frac{\mu_5}{\mu}\right)^{\frac{2}{3}} \qquad \text{Equation 26}$$

where μ_5 is the viscosity of the water at +5 °C (1.519×10^{-4} pa s^{-1}) and μ is the viscosity of the water at +25 °C (8.9×10^{-5} pa s^{-1}). The flow velocities and directions, water levels, bed shear stress, sediment transport and morphological change derived from the modelling results were used in the analysis.

4.2.2 2D hydrodynamic modelling of paper III

In paper III, a 2-dimensional hydrodynamic simulation was performed according to equations 7-11. The model was run over the spring flood of 2009 was performed to derive the spatial and temporal distribution of the hydraulic processes over a meander bend for a structured grid of 2 m x 2 m cell size. In this paper, the simulation was realised using the TUFLOW model. Spatially varying Manning's roughness coefficients were defined according to the surface material and adjusted in the calibration process. The spatial and temporal variation of flow depth and velocity were extracted from the modelling results, and stream power was calculated according to equation 3.

4.2.3 2D hydrodynamic and sediment transport modelling of paper IV

In paper IV, a 2D hydrodynamic model with sediment transport but without morphological changes was run over the spring flood of 2013 using the Delft3D model. The hydrodynamic simulation was equivalent to the 2D model in paper II and the van Rijn (1993) transport algorithm (equations 17-24) was used to model the sediment transport. In the calibration process, the modelled water levels, flow velocities and sediment transport rates were matched to the field measurements. The hydrodynamic model was calibrated by adjusting the horizontal eddy viscosity and diffusivity coefficients and Chezy's roughness coefficient. The sediment transport rate was calibrated by adjusting the parameters f_{sus} and f_{bed} in equations 17 and 22, respectively. The initial grain size distribution was based on 192 sediment samples in the field, and the point data of the median size of the sediment was interpolated over the computational grid using a triangular interpolation method. The spatial and temporal distribution of flow depth and velocity, as well as bed shear stress (equation 25) and sediment transport based on the model were used to interpret the morphological characteristics and changes over three meander bends.

5 RESULTS AND DISCUSSION

In this chapter, the main findings of the four papers of this thesis are presented and discussed. The results can be applied to sand-bed meandering rivers where the point bars are mostly exposed and inundated mainly during flood events.

5.1 Sub-bend scale flow structures of meander bends associated with flow stage

The flow structure was investigated using 3D measurements of ADCP (papers I and II) and by 2-dimensional (Papers II, III and IV) and 3-dimensional (paper II) computational models. In general, the measured and modelled location of the HVC supported the findings of many earlier studies in that it shifted from the convex towards concave bank and from near-surface to near-bed with distance downstream (e.g. Leopld and Wolman, 1960; Dietrich *et al*., 1979; Rodriguez *et al*., 2004). The results of this study also showed that the flow stage has a major impact on the flow structure and the spatial distribution of flow velocity and stream power in a meander bend (papers I, II, III and IV). Especially, the transverse shift of the HVC is controlled by the changes in the discharge and flow depth, which are usually interconnected (papers I and III). During a bankfull discharge, the flow directs through the bends, across the point bar; the HVC hits the concave bank at the downstream end of the bend (papers I and III). A decrease in depth over the point bar increases the effect of the point bar upon the flow trajectory (papers I and III), a phenomenon also noted in previous studies (e.g. Frothingham and Rhoads, 2003; Engel and Rhoads, 2012). This leads to the transverse shift of the HVC further upstream compared to high discharge (papers I and III), a result supported by findings of Hooke (1975) and Dietrich and Smith (1983). Thus, a minor difference in the discharge may denote considerably different flow velocities on certain parts of a bend (paper III). In particular, the spatial analysis in paper IV showed that the experienced flow structure over the point bar depends greatly upon the flow depth over the point bar, not only upon the discharge magnitude. In papers I and IV, the backwater effect was noted to have a significant effect on the flow structure by increasing the flow depth and decreasing the flow velocities. On areas affected by the backwater effect, the same discharge magnitude may produce very different flow velocities and flow depths depending on the strength of the backwater effect. The results of papers I and IV also indicated that the phase of the bend development influences the flow field. In a mature stage bend with high amplitude, the flow depth over the point bar remains low, and the flow is concentrated in the main channel due to the high width-to-depth ratio (paper IV). Thus, the HVC does not influence the point bar as much in mature-stage bends compared to early-stage bends (paper IV). The impact of the flow on the point bar platform has been noted to diminish in well-developed bends in previous studies as well (Hickin, 1974; Hooke, 1995; Pyrce and Ashmore, 2005). Conversely, the effect of the point bar and the bend curvature on the flow trajectory is emphasised in mature bends with high curvature.

The secondary circulation of flow has been noted to be generic for meander bends in various earlier studies (e.g. Rozovskii, 1957; Bathurst *et al*., 1977; Bridge and Jarvis, 1982; Engel and Rhoads, 2012). Three-dimensional flow fields were measured in papers I and II and modelled in paper II in this study. According to the ADCP measurements, the transverse flow was directed towards the outer bank upstream of the bend apices, downwards close to the concave bank and inwards beyond the bend apices (papers I and IV). Thus, the secondary cell was not fully developed and was weaker in Bend 4 (high curvature, 1.8) compared to Bend 3 (curvature 1.4) (paper I). According to the 3D simulation (paper II), however, the secondary cell was fully developed in Bend 3. In previous field-based studies, a distinct and clear secondary circulation cell has been observed (Bridge and Jarvis, 1976; Bathurst *et al*., 1977; Engel and Rhoads, 2012). Other studies have shown the secondary circulation to

strengthen with increased bend curvature, however, saturating in sharp bends (e.g. Blanckaert, 2009; Ottewanger *et al*., 2012), and increasing in strength in proportion to discharge, but diminishing in very high discharges (Bathurst *et al*., 1979) and not forming at all with a large width-to-depth ratio (Leopold and Wolman, 1960; Termini and Piraino, 2011). In meandering channels, the width-to-depth ratio often increases with increasing discharge and depth. According to paper I, the secondary circulation weakened as the flow depth decreased. Further, it seems that a sufficient flow velocity is required for the secondary circulation to develop, and, similarly to the shift of the HVC, the circulation occurred further upstream with lower discharges (paper I), indicating a strong dependence on the point bar morphology. Thus, combining the results of this study with earlier findings, it seems that the strength of the secondary circulation is a product of many factors interacting over a meander bend: the point bar and bend morphology together with the flow velocity and depth introduce complex interactions leading to various flow structures in natural channels, which cannot yet be explained fully with the existing theories. Even though valuable new insights to the governing factors can be gained in simplified laboratory channels (e.g. Blanckaert, 2009; Ottewanger *et al*., 2012), this study showed that field investigations are necessary to fully understand the processes and their various modes in nature.

The outwards flow throughout the water column has also been noted in previous studies to occur at the upstream part of the bend due to the shoaling of the flow over a point bar (e.g. Dietrich and Smith, 1983). The impact of point bar upon the flow also affects the secondary circulation: with decreasing discharge, the secondary circulation cell occurs further upstream (paper I). In previous studies, the strength of the secondary flow has also been noted to depend upon the flow stage: the decrease in flow depth caused the secondary currents to diminish (Hooke, 1975; Ferguson *et al*., 2003). However, some studies have shown that the secondary flow is strongest at medium discharges (Bathurst and Thorne, 1979). The results of the current study also indicate that the flow stage has an impact on the intensity and location of secondary circulation in a meander bend, but there is not enough evidence to draw any specific conclusion on the process. Further, the measured or modelled 3-D flow fields of this study did not show clear evidence of outer bank circulation cell, reported in many field studies (e.g. .g. Bathurst *et al*., 1979; Thorne *et al*., 1985). However, as this study focused on the processes over the point bars, the outer banks were not dissected with high detail. The secondary flow structures in natural meandering channels and their dependence on the bend morphology and flow stage need further research, as the secondary flow has a major impact on the meandering river evolution.

Few detailed investigations of the spatial distribution of the flow velocities over a meander point bar with changing discharge have been implemented prior to this study (see Bathurst *et al*., 1977; Dietrich *et al*., 1979; Dietrich and Smith, 1983; Hodskinson and Ferguson, 1998; Ferguson *et al*., 2003). According to the results of the current study, the point bar platforms experience low inundation periods during a flood event, but, as they are inundated during the high discharges, they experience high flow velocities (papers I, III and IV). The hydrodynamic models of papers III and IV also showed that the point bar margins are characterised with long inundation periods that include both high and low discharge periods and stream powers. In addition, the bar margin area beyond the apex is often affected by a recirculation of flow (a weak reverse flow) (Rozovskii, 1957; Frothingham and Rhoads, 2003; Ferguson *et al*., 2003), which, according to the results of the current study, does not require secondary circulation to occur, but a sufficient, not too shallow, not too deep, flow stage over the point bar (paper I). The bar head area experiences very high stream powers and is affected by the HVC during high discharges (papers I, III and IV). It also depends upon the bend upstream as the location of the HVC may be strongly affected by the previous bend (paper IV). The stream power and flow velocity over the point bar tail are mostly low relative

to the flow depth. They depend greatly on the location of the HVC, which may flow over the bar tail during high discharges, but shifts towards the outer bank as the discharge decreases. This was noted in all of the thematically focused papers of this study (papers I, III and IV). The recirculation of flow also decreases the stream power over the bar tail (papers I and III). The flow field over the bar head and bar tail are especially affected by the transverse shift of the HVC (paper IV).

5.2 Spatial patterns of the flow-sediment interaction within a meander bend

According to the analysis of paper IV, the flood event plays a key role in the channel evolution in Arctic and sub-Arctic meandering rivers, with significant annual flood events, unlimited sediment availability and exposed point bars for most of the year, by being responsible for the changes in the point bars. Furthermore, the bend and point bar morphology itself has a notable impact on the experienced morphological changes over the bend. This agrees with the studies by Gautier *et al*. (2010) and Hooke and Yorke (2011). A long-term scale study by Hooke (2008) also showed that the river geometry is highly responsive to the experienced flow structure during a flood event. According to the results of this study (papers I, III and IV), the annual variation in the sediment budgets of one point bar can be considerable. Similar remarks have been made in other field studies as well (e.g. Gautier *et al*., 2010; Hooke and Yorke, 2011). Furthermore, the net changes of a point bar are not clearly interconnected to the peak discharge magnitude, but the duration of a certain discharge seems to play a more important role (paper I, II and IV). This is consistent with the finding of Rinaldi and Darby (2008), who stated that the magnitude of erosion depends on the duration of the competent flow. Also, Asselman and Middelkoop (1998) noted that the spatial variability of erosion and deposition over study areas along the Rhine and Meuse rivers, Netherlands, depend on flood magnitude and duration. Lotsari *et al*. (2014b), however, stated that the area of net deposition over point bars is larger with higher spring-flood discharge magnitude. The detailed LiDAR-based change detections of this study showed that impacts of a certain discharge or flow stage of particular duration, however, cannot be interconnected to the net erosion and deposition on a whole point bar. However, the point bars consist of different units, which have varying responses to a certain flow. The morphological changes caused by previous flood events also affect the experienced erosion and deposition caused by the following flood (papers III and IV). The same phenomenon has been noted in other study sites as well (Gautier *et al*., 2010). In addition, the study area is influenced by the backwater effect, which considerably modifies the experienced erosional forces caused by a certain discharge (papers I and IV).

In addition, the spatial patterns of the net erosion and net deposition caused by a certain flood event vary considerably between point bars within a reach (papers I, II, III and IV). Similarly, Hooke (2007) showed that there is no clear association of changes in one bend with another. Results of paper IV indicated that usually each part of a point bar experiences both scour and fill during one flood event. Whether net erosion or net deposition occurs in one part of a point bar depends on at least: the relative differences in stream power, cross-stream flow components, flow depth and flow velocity and duration of each discharge, grain size distribution and the shape of the bend and bar, i.e. the stage of the bend development (papers I and IV). Also, the magnitude of the sediment transport and the net morphological change over a certain part of a point bar are not interconnected: areas of net erosion and deposition may have experienced either high or low sediment transport rates during the flood event (paper IV).

Based on the temporal analysis of the erosional and depositional processes in papers III and IV, erosion occurs during high discharge and deposition during the falling and low

water stage. Thus, the period of the moderate discharges during the flood's descent has a major impact on the point bar accretion. Lotsari *et al*. (2014b) stated that the longer the point bar is submerged, the more likely it is that it experiences net deposition. The results of this study are partly contradictory to their statement. Based on the results of this study (papers III and IV), it seems that, instead of an entire point bar, a certain part of a point bar is more likely to gain net deposition, the longer it is inundated. Thus, the share of net deposition of a point bar is strongly dependent on the point bar morphology. The transverse shift of the HVC also plays a very important role in the erosional and depositional processes, as it determines the distribution of the erosional forces (papers I and III). Especially, the processes over the point bar head are interconnected to the shift of the HVC, which is dependent on the flow stage (paper I). Thus, even though many studies and conceptual models of meander development (McGower and Garner, 1970; Hooke, 1975; Gautier *et al*., 2010) state that the point bar head is an area of net erosion, the results of this study show that as the discharge decreases, the outward shift of HVC reduces the stream power over the bar head, enabling filling to occur over the bar head during moderate and low discharges (papers I and III). Thus, the duration of certain (moderate) flow stages in relation to the point bar head elevation may significantly increase the point bar head accumulation. The bend upstream also influences the flow trajectory and affects especially the morphological changes of point bar head (paper IV). The findings of Pyrce and Ashmore (2005) support the results of the current study.

According to this study, point bar margins mostly experience net deposition (papers I, III and IV). They are also under high flow depths and stream powers during the flood, which indicates that the deposition occurs during low flow period of descending discharge, which lasts relatively long over the vertically low point bar margins (paper IV). The bar margin deposition also seems to be independent of the phase of the bend development (papers I and IV). The 3D flow field measurements of paper I showed that the point bar margin beyond the apex is especially likely to gain net deposition due to the transverse shift of the HVC with decreasing discharge, the inward near bed flow and the recirculation zone. This is consistent with many previous studies and conceptual models of meander development (e.g. Hickin, 1974**;** Bridge and Jarvis, 1976; Dietrich and Smith, 1984; Ferguson *et al*., 2003; Gautier *et al*., 2010). Net erosion is, however, also possible at the downstream part of the point bar margin given that the flow depth over the point bar is high enough to inhibit the secondary circulation and transverse shift of the HVC and that the duration of the moderate flows are short enough (paper III). The results of the current study are partly contradictory to the conceptual models of meander development in that the emphasis of the bar margin deposition shifts from downstream to upstream of the apex as the bend develops (e.g. Hickin, 1974; Hooke, 1995; Pyrce and Ashmore, 2005). In this study, major net deposition occurred also upstream of the apex on the bar margin, independent of the stage of the bend development (paper I and IV).

By contrast, the results of paper IV, in which the morphological changes of three point bars were examined, suggested that the stage of the bend development seems to control the morphological changes over the point bar platform. In mature bends, the morphological processes are concentrated at the point bar margins (paper IV), while the platforms of bends of the early stage may experience notable erosion (papers I and IV) or deposition (paper II) as a consequence of a flood. The position of the HVC, which is also dependent on the bend and point bar shape, controls the point bar platform processes (paper III). Based on the results of this study, it can be stated that the top of the point bar may experience erosion even with relatively low discharge or, by contrast, deposition during high discharge (papers I, II, III and IV). The shape of the point bar and the experienced water level play very important roles in the point bar platform development (papers I and IV). The shape of the point bar may enhance the erosion by enabling the gravitational force to intensify the sediment transport

towards the pool, or the backwater effect may increase the flow depth over the point bar, decreasing the flow velocities and enabling a filling event on the top of the point bar (paper I). Previous studies have also given unclear and contradictory results of the point bar platform development. Many studies have stated that there is a fining upwards sequence on the grain size distribution over a point bar (Bridge and Jarvis, 1976; Dietrich and Smith, 1984), while other studies have shown that coarse grains are typical for chute fill (McGowen and Garner, 1970). In the current study, both coarse and fine grains were found on the bar platforms independent of whether the area experienced net erosion or deposition. Thus, it can be expected that the scour and fill will have an oscillation at the platform, although it will depend on the flow stage and stream power. The morphological changes and grain size distribution based on the previous flood event play important roles in the point bar platform morphodynamics (paper I). Clear chute channels were not observed in the current study, even though they have been noted to develop in the study area based on previous studies (Alho and Mäkinen, 2010).

In previous studies, the point bar tail is almost unquestionably considered as an area of net deposition (Leopold and Wolman, 1960; McGowen and Garner, 1970; Jackson, 1976; Thompson, 1986). The identified reasons are the secondary circulation, shift of the HVC and the recirculation at the inner bank (Dietrich and Smith, 1983). In addition, the sudden increase in flow depth after the point bar crest decreases the experienced stream power over the bar tail, enhancing the filling further (McGowen and Garner, 1970; Dietrich and Smith, 1983). The results of the current study, however, showed rather varying morphological changes over the bar tail areas (papers I, II and IV). Even though the net deposition dominated the bar tails, the deposition was often concentrated only on the bar tail margin (papers II and IV). The formations over the bar tails seem to be notably dependent on sufficient water levels relative to the point bar height (paper IV), and the scroll bars over the bar tail require secondary circulation to develop (paper I). Thus, the local planform characteristics, including the shape of the bend upstream, affect the bar tail evolution (paper IV).

Altogether, the results of this study agree with the recent field-based studies of Gautier *et al*. (2010) and Hooke and Yorke (2011) in that the point bar and bend morphology itself modifies the experienced fluvio-morphological processes over the point bar and bend. The spatial distribution of the morphological changes seems to depend both on flow depth and velocity and the duration of certain flow conditions, consistent with Middelkoop and Asselman (1998).The effect of the sediment supply and sediment pulses from upstream and its timing relative to discharge magnitudes most likely have an effect on the meander bend morphodynamics during a flood (Lane *et al*., 1996). However, as the sediment transport rates in this study were mainly based on the hydraulic model, the estimations of the sediment transport variation in space and time were not reflecting the actual sediment supply or transport pulses. Continuous sediment transport measurements with sufficient spatial resolution should be performed in order to fully discuss the subject. This, however, would require a large number of samples and would therefore be extremely labour-demanding (c.f. Gomez *et al*., 1990).

5.3 New perspectives to fluvial geomorphology of meander bends provided by close-range remote sensing methods

State-of-the-art, close-range remote sensing methods were exploited in this study in collecting topographical and bathymetric data and in flow field and discharge measurements. In paper IV, the use of the UAV-based ortophotos was also piloted in fluvio-geomorphological interpretation. In each of the papers of this study, the morphological

changes over the meander point bars were measured using TLS and MLS. The results of this study provided extensive demonstration of the advantages of TLS and MLS in meso-form scale determination of fluvial formations, morphological changes and sediment budget in a naturally meandering river environment. Even though the infrared-wavelength LiDAR is not water penetrating, often large areas can be surveyed during low water periods with high precision using TLS and MLS.

Different MLS setups used in this study enhanced notably the spatial coverage of the TLS data and enabled measuring of relatively large areas in a reasonable amount of time. Efficiency in data collection is important in fluvial geomorphology, as the changes in riverine environments may be quick; there is often a negative relationship between scale of change and rapidity of change (Knighton, 1998). Average MLS point densities of 500-7400 points/m^2 (paper I) was achieved in this study with the MLS approaches, depending on the approach used (i.e. BoMMS or CartMMS). The reach covered by the MLS survey in the current study is more than 2 km long and consists of 5 meander bends with exposed point bar areas between 3500 and 16000 m^2.The achieved data densities were notably higher compared to those typically achieved with ALS (5–50 points/m^2, e.g. Höfle *et al*., 2009; Vosselman and Maas, 2010) or alternative field measurement techniques. For example, Brasington *et al*. (2000) surveyed a reach of 200 x 80 metres in size with a point density of 1.1 points/m^2, while Fuller *et al*. (2003) achieved a point density of ~0.06 points/m^2 using total station in an area of ~20 000 m^2. In paper IV, the use of MLS allowed for investigation of three bends, which enabled comparisons between bends in different phases of development.

Due to the high spatial resolution and accuracy of the collected LiDAR data, very detailed interpretation of the spatial patterns of the net erosion and deposition as well as fluvial formations was possible. DTMs of 0.1 to 0.25 m^2 cell sizes were produced based on the LiDAR point clouds. The importance of the spatial coverage and accuracy of the geometrical data has been noted in many previous studies (e.g. Brasington *et al*., 2000; Bates, 2004; Heritage and Hetherington, 2007; Alho *et al*., 2009b) and the crucial nature of the high vertical precision is emphasised when computing morphological change volumes based on DoD (Brasington *et al*., 2003). The traditionally used cross-sectional measurements of the river geometry (e.g. Dietrich and Smith, 1983; Ferguson and Ashworth, 1992; Warburton *et al*., 1993; Frothingham and Rhoads, 2003;) and DEMs produced with more traditional methods, often presuming a trade-off between spatial extensiveness and spatial resolution (Lane *et al*., 1994; Heritage *et al*., 1998; Brasington *et al*., 2000; Fuller *et al*., 2005), may lead to a discontinuous picture of the river reach and maybe to an incorrect interpretation of the phenomenon (Heritage and Hetherington, 2007). In this study, meso-form scale formations, such as dunes, chute bars and scroll bars were observed from the LiDAR-based DTMs (papers I, II and IV). In paper I, the level of detail in the change detection, based on MLS data, was approximately ~0.1 metres, and the vertical RMSE of the DTMs was less than 0.05 m. As the quality of the MLS measurements is mainly limited by the accuracy and quality of the GPS measurements, the MLS data resolution was not sufficient for micro-form scale analysis of meander bend fluvio-morphology (paper IV).

The laser scanning technique allows for measurement of areas that are difficult to achieve using traditional methods or, for example, GPS, as it does not require physical contact with the measured object. Therefore, it also minimises the measurement errors caused by the disturbance of the measurement equipment or the measurer entering the study site. The BoMMS used in papers I, III and IV provided a practical scanning angle for surveying the river banks and vertical parts of the channel. The main limitation of the infrared wavelength laser scanners is that it cannot be used in bathymetric surveys (cf. Williams *et al*., 2014). Furthermore, the laser scanning campaign is dependent on the weather conditions, as the scanners cannot be used in the rain**.** The advantages of the TLS and MLS have been noted,

and the approaches have been exploited to some degree in previous studies of fluvial geomorphology (e.g. Heritage and Hetherington, 2007; Milan *et al*., 2007; Morche *et al*., 2008; Hodge *et al*., 2009; Heritage and Milan, 2009; Brasington *et al*., 2012).

In addition, the high resolution measurements of the river geometry enabled building of detailed computational reconstructions (papers II, II and IV). In paper II, the LiDAR-based change detection over the point bars was also used to assess the functionality of a morphodynamic model. The bathymetric measurements for the initial geometry of hydraulic models were carried out using side-scanning sonar (paper II), single-beam sonar attached to a rubber boat (paper III) and an ADCP sonar attached to a remote-controlled boat (paper IV). The remote-controlled boat enabled bathymetry measurements on shallow areas without disturbing the river bed (paper IV). Due to lower spatial resolution of the bathymetric data (point spacing varied between 0.25 m and 2m) compared to the topographical data, no change detection was realised over the areas that were continuously inundated. The bathymetric surveys often suffer from lower spatial resolution and accuracy compared to the topographical surveys (e.g. Brasington *et al*., 2003; Westaway *et al*., 2003). The point densities achieved with the remote-controlled boat in paper IV (point spacing of 1-2 m) could be improved, but the time required for executing the survey increases in proportion to the spatial resolution achieved. The side-scanning sonar enables better spatial resolution (point spacing of 0.25 m in paper II) in significantly shorter time but requires more flow depth (e.g. Parsons *et al*., 2005; Kaeser *et al*., 2013). There have also been attempts to develop new methods that would enhance the bathymetric data resolution and density by using, for example, optical methods (e.g. Legleiter, 2012; Flener, 2012; Williams, 2014). Accurate and dense bathymetric measurements, combined with the LiDAR-based topographical data, should be used in the future in comprehensive change detections that would cover the entire river channel and also in assessing the computational model functionality.

The ADCP was exploited in this study also to measure the discharge (papers I, II, III and IV). It allowed for a rapid and reliable discharge measurement and thereby building of discharge rating curves with increased reliability (e.g. Oberg and Mueller, 2007). In paper I, the discharge was measured during 10 different flow stages with ADCP. In paper I, the 3D flow field measurements using ADCP during three flow stages enabled linking the morphological changes to the complex flow field of two river bends. The ADCP technique is especially functional when doing measurements in rapidly changing discharge as it is more rapid to use compared to ADV, for example (e.g. Engel and Rhoads, 2012). Thus, it enables the 3D flow field mapping without the discharge changing (paper I). It also enables detailed flow field measurements in deep waters (compare to ADV, e.g. Rehmel *et al*., 2007). The ADCP and ADV techniques have been exploited in many previous studies, which has provided new insights into riverine processes for decades now (e.g. Simpson *et al*., 1990; Claude *et al*., 2014). However, achieving a high spatial resolution of the flow data is rather time consuming, and covering large areas without discharge changing may thus still be impossible in the field, even though attempts have been made to map the flow field in high resolution with spatially continuous ADCP data (cf. Williams *et al*., 2013; Flener *et al*., submitted manuscript). Thus, a continuous record of the flow structure over a river reach with changing discharge cannot yet be produced in natural environments using the current field measurement techniques (paper IV).

In paper IV, a study approach combining detailed field measurements (GSD, observations of formations, RTK-GPS measurements), remote sensing (MLS, TLS, UAV-based aerial photographs) and computational modelling (2D CFD with sediment transport) was exploited. Based on the results of paper IV, combined study approaches are highly recommended in fluvial geomorphology because the methods complement each other. The close-range remote sensing provides accurate data over large areas, and the temporal

resolution may be enhanced using computational modelling. The interpretation of the LiDAR-based DTMs over the point bars was improved using a low altitude photomosaic of the UAV. The UAV enables collection of very high resolution (grid resolution of 0.05 m in this study) geo-referred aerial photographs. UAV-based aerial photographs have not been applied to any large extent in fluvial geomorphology thus far. The high-resolution aerial photography proved to be practical in improving and confirming the analysis made based on the LiDAR data. However, the full potential of the UAV-based high-resolution aerial photographs should be exploited and investigated in the future. Based on this study, for example, the supporting field observations would enhance the interpretation of the photographs. Therefore, based on this study, field observations are still necessary when studying natural environments and cannot be replaced fully using close-range remote sensing methods.

5.4 CFD in investigation of a natural curved channel

The results of papers II, III and IV provided an insight on the weaknesses, strengths and possibilities of CFD in the fluvio-geomorphological analysis of a natural river. According to this study, CFD allows for spatial and temporal resolution of flow and sediment transport data, unachievable by field measurements (papers II and IV). They are therefore extremely suitable in supporting and enabling fluvio-geomorphological analysis of natural environments and over remote areas, where continuous measurements of flow and sediment transport is not possible (papers III and IV). However, their representativeness in natural rivers should be ensured with field measurements, and the user should understand the simplifications present in the simulation results (paper IV). Furthermore, the spatial resolution of the simulation results depends on the resolution of the boundary data. In this study, CFD were applied in a naturally meandering river, and the boundary conditions were based on the field measurements of flow and morphology. CFD were used in papers II, III and IV to simulate the flow field over the study area during the entire flood event. In papers II and IV, the prevailing sediment transport rate was also simulated based on the hydrodynamic calculations and measured grain size distribution. In paper II, the changes in the bed level caused by the sediment transport were simulated and compared with the actual changes measured in the field.

A 2D model was applied in each case. In paper II, both 2D and 3D models were used to model the flow and morphodynamics. The models' sensitivity of various user-defined parameters was tested and the results of the 2D and 3D simulations were compared with each other and with detailed field measurements to assess their functionality. Based on the comparisons, a 3D hydrodynamic model is preferred when investigating the flow characteristics in a meander bend, because many flow features of curved channels, such as secondary flow and vertical location of the HVC, can only be simulated with a 3D model. The 2D model, however, produced the depth-averaged flow field satisfactorily. In paper III, the depth-averaged model was not able to model the flow separation at the inner bank beyond the apex. The shortages of the 2D model are emphasised downstream of the apex, as noticed also in previous studies (Alho and Mäkinen, 2010), where, for example, the near-bed inward flow plays an important role in the point bar deposition. For example, the scroll bar formation is a consequence of the three-dimensional flow field (paper III). Also, Rodriguez *et al*. (2004) stated that a 3D approach is required when simulating complex flow structures such as transverse velocity components, helical flow, the recirculation zone and the submergence of an HVC. Even though the depth averaging was noted to have a significant effect on the erosional power of the flow (e.g. bed shear stress), there was no notable difference between the 2D and 3D morphodynamic reconstruction over the same flood event (paper II). The

turbulence closure model used in the 3-D simulation (i.e. standard k-ε model) may not be the most reliable approach for estimating the turbulent fluctuations, which, in turn, affect the sediment transport patterns. Previous studies for example by Rodriguez *et al*. (2004) and Bradbrook *et al*. (1998) have shown that the RNG k-ε model, which is a more sophisticated version of the standard k-ε model, performs better in recirculation regions and regions with high shear. The RNG model should, therefore, be applied in the future in curved channel reaches and to clarify the different factors involved in the morphodynamic models performance. Further, applying a fully 3D model, instead of the quasi-3D approach applied in this study, could improve the modelling results and thereby highlight the differences between the simulated morphodynamics of 2D and 3D models.

The results of papers II, III and IV indicated that the 2D hydrodynamic model provides a well-functioning tool for estimating the main flow distribution over large areas and over changing discharge with high spatial resolution, but it should be used with caution in a curved channel environment. In addition, it requires notably less computational power compared to the 3D approach. CFD also provide a convenient tool for estimating the sediment transport rates over a large area with high spatial and temporal resolution given that sufficient calibration data of the sediment transport rate is available (papers II and IV). Modelling the short-term morphological changes, however, has major uncertainties, which are related to difficulties in calibration and validation as well as to the correct determination of the user-defined parameters (paper II). In a natural environment, there also are various unpredictable phenomena, such as runoff and sediment supply changes, which cannot be taken into account in a simulation without detailed field observations but which may have a notable effect on the modelled morphodynamics.

The models` (2D hydro- and morphodynamic models) sensitivity to many user-defined parameters was tested in paper II. Based on the sensitivity analysis, the roughness parametrisation influences the spatial distribution of flow velocities and thereby the morphodynamics as well. When using the Chezy roughness, the roughness height is related to water depth (Equation 13 in paper II). When a uniform Chezy roughness is applied over the whole modelling area, the roughness height over the point bars remains lower compared to the pools. Based on the sensitivity analysis of paper II, this leads to lower point bar height and smaller pool depth compared with other roughness parametrisation methods. Even though the effect of the roughness parametrisation on the simulated morphodynamics has not been studied much before, some previous studies have also stated that it has a significant effect on bed morphology (Nicholas, 2003; Lesser *et al*., 2004; Schuurman *et al*., 2013).

The grain size parametrisation, used as the initial sediment size in the morphodynamic model, is critical when simulating the morphological changes in naturally meandering rivers (paper II). This has been noted in many previous studies and in various environments (e.g. Nicholas, 2000; Pinto *et al*., 2006; Papanicolaou *et al*., 2008; Nicholas, 2013; Lotsari *et al*., 2014a). Also, the transverse bed slope effect parametrisation and the selected sediment transport relation have a notable effect on the morphodynamics. The simulated transport rates with the two algorithms tested in this study (Engelund and Hansen, 1967 and van Rijn, 1993) were pronounced with high discharge and flow velocities. The exclusion of secondary flow did not have much of an effect on the point bar morphodynamics in the test simulation of paper II. The simulation period of one flood event (17 days) is, however, too short to make a comprehensive conclusion on the importance of the secondary flow correction to the curved channel morphodynamics. Based on the results of paper II, though, the grain size parametrisation, transverse bed slope effect and sediment transport relation have more of an effect on the modelled bed level changes compared to the secondary flow correction in the 2D approach. The co-effect of the parameters was not tested, but it seems that especially the chosen sediment transport relation might affect the impact of the other parameters. For

example, the suspended load is not modelled separately in all of the transport relations (e.g. Engelund and Hanasen, 1967). In that case, the underestimation of suspended load transport would directly diminish the importance of the secondary flow correction, as the secondary currents mostly transport the suspended load. The modelled bed load transport rate, on the other hand, is strongly related to the transverse bed load effect (Nicholas, 2013).

6 CONCLUSIONS AND DIRECTIONS FOR FUTURE RESEARCH

This study contributes to improving the understanding of the sub-bend scale fluvio-morphological processes over meander bends, with special emphasis on point bars, by exploiting a combined approach of conventional field measurements, close-range remote sensing and computational fluid dynamics. Mainly, the results of this study follow well the existing theories and results of previous studies. However, the improved spatial and temporal resolution of the data provided some new insights to the flow-sediment interaction in a natural sand-bed meander bend. This study also demonstrates the advantages and limitations of various modern technologies in fluvial geomorphology and indicates the future directions. The main conclusions of this PhD thesis are the following:

1. This study was implemented in a sand-bed meandering river, in which point bars are inundated only during the snow-melt-induced spring floods, and the sediment availability is unlimited, originating from the glacio-fluvial deposit. The spring flood events play an important role in deforming the meander bends over the reach, and they are especially responsible for the morphological changes over the point bars, which, in turn, affect the fluvial geomorphology of the entire bend. Based on this study, it can be stated that the spring flood events have a notable contribution in the meander evolution in such meandering rivers in sub-Arctic and Arctic areas. Therefore, climate change, which has been reported to influence the flood regime in Arctic areas (Lotsari *et al*., 2010; Vejalainen *et al*., 2010), may have a notable influence on the dynamics of meandering rivers in Arctic areas.

2. The flow structure over a meander bend depends greatly upon the flow depth over the point bar, not only upon the discharge magnitude. Thus, the bend and point bar morphology, and thereby the phase of the bend development, also affects the flow structure. An increase in flow depth decreases the effect of the point bar on the flow trajectory, influencing the location of the HVC and secondary circulation. The shift of the HVC from inner bank to outer bank also occurs further upstream in mature bends with high amplitude and curvature. Thus, the HVC does not influence the point bar as much in mature, compared to early stage bends. The experienced flow strength over the bar head and bar tail are especially dependent on the transverse shift of the HVC. In the very low water stage and with high width-to-depth ratio, as well as low flow velocities, the secondary circulation may not be able to develop. The dependence of the strength of the secondary circulation on the bend curvature and discharge characteristics seems to be a more complex subject; the various forms of secondary circulation in naturally meandering channels need further research.

3. The net morphological changes of meander point bars are not directly related to the peak discharge magnitude, but the durations of influential discharges and water levels seem to play a more important role as point bar and channel modifiers. In general, erosion occurs during high and deposition during the falling and low flow stage. The impacts of a certain discharge or flow stage of particular duration, however, cannot be linked to the sediment budget of the entire point bar. However, the point bars consist of different units, which have varying responses to the flow stages. The spatial patterns of erosion and net deposition caused by a certain flood event may also vary considerably between point bars within a reach as the point bar and bend shape modifies the experienced flow patterns:

- The transverse shift of the HVC affects the fluvio-morphological processes over the point bar head. During the flood's descent, the duration of certain (moderate) flow stages in relation to the point bar head elevation may significantly increase the point bar head accumulation leading to net deposition, which is contradictory to conceptual models of meander development, according to which the point bar head is an area of net erosion. Also, the shape of the bend upstream affects the bar head evolution by controlling the flow trajectory over the bar head.

- Point bar margins experience mostly net deposition as a consequence of flood events. As they experience high flow depths and stream powers during the high discharges, the deposition occurs mostly during a relatively long-lasting period of low discharge and velocity on the vertically low point bar margins. No clear connection between the stage of the bend development and the morphological changes over the bar margins can be found based on this study, which is contradictory to the conceptual models of the meander bend development (e.g. Hickin, 1974; Hooke, 1995; Pyrce and Ashmore, 2005). However, in mature bends, the morphological processes are focussed over the point bar margins.

- Only minor morphological changes occur over the point bar platforms of mature meander bends, while the platforms of early stage bends may experience notable changes as a consequence of a flood. The shape of the point bar and the experienced water level relative to the elevation of the point bar platform play very important roles in the point bar platform development.

- Also, the morphological changes and formations over the bar tails seem to greatly depend upon the influential water level relative to the point bar height. The bar tails may experience both net erosion and net deposition as a consequence of a flood, independent of the peak discharge magnitude. This differs from the findings of many previous studies. The transverse shift of the HVC and the recirculation at the inner bank are responsible for the filling over the bar tail. Secondary circulation is not required. The scroll bars over the bar tail, however, require secondary circulation to develop. Thus, the local planform characteristics and the shift of the HVC towards the convex bank with distance downstream with decreasing discharge play important roles in the bar tail fluvio-morphodynamics.

4. Close-range remote sensing techniques (MLS, TLS, ADCP, echo sounding, UAV) provide accurate, spatially efficient and objective ways of measuring the fluvial forms and processes in rapidly evolving riverine environments. They also allow for surveys without disturbing the measurement target. Mobile terrestrial laser scanning enhances notably the spatial coverage and temporal efficiency of the TLS, still allowing for very high point densities (500-7400 points/m^2 in this study) and absolute vertical accuracies (RMSE 0.013-0.051 m in this study) compared to traditional terrestrial survey methods or airborne laser scanning. The ADCP allows for rapid 3D flow field measurements and is thus valuable in rivers with rapidly changing discharges. The measurements can be used in fluvio-morphological analysis and in assessing the functionality of hydrodynamic models. However, spatially coverage flow field measurements over a large area cannot yet be realized with ADCP. In addition, the data acquisition efficiency and achieved spatial resolution of the bathymetric measurements is not yet competitive to the terrestrial survey methods but need further development.

5. Computational fluid dynamics are suitable and efficient approaches in fluvio-geomorphological studies of natural rivers in enhancing the spatial and temporal resolution of flow and sediment transport data. They are especially practical in studies of remote areas, where continuous measurements of flow and sediment transport are not possible to implement. The reliability of the modelling results depend, at least, on the model dimension, quality of the boundary and input data, the user-defined parameters and the chosen sediment transport algorithm. The achievable resolution of the simulation results depend upon the boundary data resolution and computational power. A 3D hydrodynamic model should be preferred when investigating complex flow structures of a meander bend. The secondary circulation was, however, overemphasised by the 3D simulation performed in this study. A 2D hydrodynamic model is a suitable tool for simulating the main flow distribution and sediment transport with high spatial and temporal resolution. The depth-averaged results of the curved channel environment should, however, be interpreted with caution. CFD may also be used in estimating the sediment transport rates, if calibration data is available. Simulation of short-term morphological changes, however, has major uncertainties related to, for example, a correct determination of the user-defined parameters of the model. The parametrisation of the grain size plays an especially important role. Also, the transverse bed slope effect and the used sediment transport relation affect the modelled bed level changes.

6. A study approach combining various methodologies is fruitful in fluvial geomorphology. A combination of conventional field measurements and observations, close-range remote sensing and computational modelling enables a detailed fluvio-geomorphological analysis over relatively large areas in natural riverine environments and thereby provides potential to deepen the understanding of the fluvial processes. The close-range remote sensing techniques allow for rapid and accurate surveys of river geometry, distribution of fluvial forms and flow characteristics. The computational fluid dynamics provide a unique way of observing a wide range of fluvio-morphological processes in three dimensions with spatial and temporal resolution unachievable with field measurements. Conventional field measurements and observations are, however, still mandatory when investigating a natural river environment. The opportunities of these approaches and their combinations has not yet, however, been utilised to a wide extent in fluvial geomorphology. In particular, the processes in natural environments, which, in the end, are the focus of the scientific work, can be studied with completely new precision in the future by combining field observations, close-range remote sensing and computational modelling.

Surveying morphological changes with the precision presented in this study over several years and flood events and including detailed bathymetric measurements in the time series will definitely increase the understanding of the meander bend fluvio-morphology and the important factors involved in it. Thus, longer time scale measurements and modelling would be important in the future. Subjects that need further research include the effects of turbulence, secondary flow structures, sediment transport and sorting, vegetation and the processes over a whole catchment to the meander dynamics in natural environments. These could be approached with completely new precision and spatial and temporal resolution by exploiting a combined study approach of field observations, close-range remote sensing and computational modelling. Furthermore, the impact of snow and ice cover in the meander and point bar dynamics over sub-Arctic and Arctic areas is an important subject of future research. For example, ADCP can be used in sediment transport measurements (cf. Dinehart and Burau, 2005a; Merckelbach, 2006; Rennie and Church, 2010), in flow field mapping

over large areas (cf. Guerrero and Lamberti, 2011), as well as in observing turbulent fluctuations (Gargett, 1994; Nystrom *et al*., 2007), secondary currents (Dinehart and Burau, 2005b) and detecting changes in river bed (Dinehar and Burau, 2005a). Even though these methods have been demonstrated and assessed in the literature, the application of such approaches in fluvial geomorphology is still limited (cf. Parsons *et al*., 2007). In the meander bend environment with high spatial variability of flow velocities and sediment transport, efficient field mapping is highly recommended in the future. Mobile laser scanning will enable mapping the changes in the riverine topography with very high accuracy and spatial resolution. The efficiency and resolution of the bathymetric data should be improved and detailed change detection realized over the inundated areas as well. With these detailed measurements, more reliable computational reconstructions of natural river channels also can be built over large areas, an objective that will open a countless amount of new opportunities in fluvial geomorphology. The calibration and validation of hydro- and morphodynamic models of long time periods and over many meander bends with different planform characteristics should be pursued in order to increase their reliability and to point out the limitations. ADCP and MLS will provide functional and efficient data collection methods for that purpose. Further, a more sophisticated turbulence closure model (for example the RNG k-ε model) should be applied in modelling the turbulent fluctuations in curved channels. At the same time, more investigation is needed of the models' sensitivity to user-defined parameters, their spatial variability and their different combinations in different natural environments.

REFERENCES

Ackers P, Charlton FG. 1970. Meander geometry arising from varying flows. Journal of Hydrology 11: 230-252.

Alho P, Kukko A, Hyyppä H, Kaartinen H, Hyyppä J, Jaakkola A. 2009a. Application of boat based laser scanning for river survey. Earth Surface Processes and Landforms 34: 1831–1838.

Alho P, Hyyppä H, Hyyppä J. 2009b. Consequence of DTM precision for flood hazard mapping: a case study in SW Finland. Nordic Journal of Surveying and Real Estate Research 6: 21–39.

Alho P, Baker V, Smith LN. 2010. Paleohydraulic reconstruction of the largest Glacial Lake Missoula draining(s). Quaternary Science Reviews 29: 3067–3078.

Alho P, Mäkinen J. 2010. Hydraulic parameter estimations of a 2D model validated with sedimentological findings in the point-bar environment. Hydrological Processes 24: 2578–2593.

Andrews, ED. 1980. Entrainment of gravel from naturally sorted riverbed material. Geological society of America Bulletin 94: 1225-1231.

Ashworth PJ, Ferguson RI. 1986. Interrelationships of channel processes, changes and sediments in a proglacial braided river. Geografiska Annaler 68: 361-371.

Asselman NEM, Middelkoop H. 1998. Temporal variability of contemporary floodplain sedimentation in the Rhine-Meuse delta, the Netherlands. Earth Surface processes and Landforms 23: 595-609.

Axelsson P. 2000. DEM generation from laser scanner data using adaptive TIN models. International Achieves of Photogrammetry and Remote Sensing 33: 111–118.

Bagnold RA. 1966. An approach to the sediment transport problem from general physics. US Geological Survey Professional Paper 422.

Bagnold, RA.1980, An empirical correlation of bedload transport rates in flumes and natural rivers: Proceedings of Royal Society London A372: 453-473.

Baker V, Costa J.1987. Flood power. In: Mayer L, Nash D (eds.). Catastrophic flooding. Binghamton Symposia in Geomorphology: international series, no. 18. Allen and Unwin, London.

Barker DM, Lawler DM, Knight DW, Morris DG, Davies HN, Stewart EJ. 2009. Longitudinal distributions of river flood power: the combined automated flood, elevation and stream power (CAFES) methodology. Earth Surface Processes and Landforms 34: 280–290.

Bates PD, Horrit M, Hervouet J-M. 1998. Investigating two-dimensional, finite element predictions of floodplain inundation using fractal generated topography. Hydrological Processes 12: 1257-1277.

Bates PD. 2004. Remote sensing and flood inundation modelling. Hydrological Processes 18: 2593–2597.

Bathurst, JC, Thorne CR, Hey RD. 1977. Direct measurements of secondaryc urrentsi n river bends. Nature, 269: 504-506.

Bathurst JC, Hey RD, Thorne CR. 1979. Secondary flow and shear stress at river bends. Journal of the Hydraulics Division 105: 1277–1295.

Bradbrook KF, Biron PM, Lane SN, RichardsKS, Roy AG. 1998. Investigation of controls on secondary circulation in a simple confluence geometry using a three-dimensional numerical model. Hydrological Processes 12: 1371-1396.

Bennett SJ, Best JL. 1995. Mean flow and turbulence structure over fixed, two-dimensional dunes: implications for sediment transport and bedform stability. Sedimentology 42: 491-513.

Bilker M, Kaartinen H. 2001. The Quality of Real-Time Kinematic (RTK) GPS Positioning. Reports of the Finnish Geodetic Institute. Masala, Finland.

Bitelli G, Bonsignore F, Unguendoli M. 2000. Levelling and GPS networks to monitor ground subsidence in the Southern Po Valley. Journal of Geodynamics 30: 355-369.

Blanckaert K, Graf WH. 2001. Mean flow and turbulence in open channel bend. Journal of Hydraulic Engineering 127: 835-847.

Blanckaert K, de Vriend HJ. 2003. Nonlinear modeling of mean flow redistribution in curved open channels. Water Resources Research 39: 1375.

Blanckaert K. 2009. Saturation of curvature-induced secondary flow, energy losses, and turbulence in sharp open-channel bends: Laboratory experiments, analysis, and modeling. Journal of Geophysical Research 114: F03015.

Blanckaert K. 2011. Hydrodynamic processes in sharp meander bends and their morphological implications. Journal of Geophysical research 116: F01003

Bluck BJ. 1982. Texture of gravel bars in braided stream. In: Hey RD, Bathurst JC, Thorne CR (eds.). Gravel-bed Rivers. Wiley, Chichester.

Bolle A, Wang ZB, Amos C, Ronde JD. 2010 The influence of changes in tidal asymmetry on residual sediment transport in the Western Scheldt. Continental Shelf Research 30: 871-882.

Booker DJ, Sear DA, Payne AJ. 2001. Modelling Three-dimensional flow structures and patterns of boundary shear stress in a natural pool-riffle sequence. Earth Surface Processes and Landforms 26: 553-576.

Brasington J, Rumsby BT Mcvey RA. 2000. Monitoring and modelling morphological change in a braided gravel-bed river using high resolution GPS-based survey. Earth Surface processes and Landforms 25: 973-990.

Brasington J, Langham J, Rumsby B. 2003. Methodological sensitivity of morphometric estimates of coarse fluvial sediment transport. Geomorphology 53: 299–316.

Brasington J, Vericat D, Rychkov I. 2012. Modelling river bed morphology, roughness and surface sedimentology using high resolution terrestrial laser scanning. Water Resources Research 48: W11519.

Brice JC. 1974. Evolution of Meander Loops. Geological Society of America Bulletin 85: 581-586.

Bridge JS, Jarvis J. 1976. Flow and sedimentary processes in the meandering river South Esk, Glen Clova, Scotland. Earth Surface Processes 1: 303–336.

Bridge JS, Jarvis J. 1982. The dynamics of a river bend: a study in 1 flow and sedimentary processes. Sedimentology 29: 499–541.

Bridge JS. 1992. A Revised model for water flow, sediment transport, bed topography and grain size sorting in natural river bends. Water Resources Research 28: 999-1013.

Bryant RG, Gilvear DJ. 1999. Quantifying geomorphic and riparian land cover changes either side of a large flood event using airborne remote sensing: River Tay, Scotland. Geomorphology 29: 307-321.

Bull WB. 1979. Threshold of critical power in streams. Geological Society of America Bulletin 90: 453 464.

Butler JB, Lane SN, Chandler JH. 1998. Assessment of DEM quality for characterizing close-range digital photogrammetry. Photogrammetric Record 16: 271-291.

Carbonneau PE, Lane SN, Bergeron NE. 2004. Catchment-scale mapping of surface grain size in gravel bed rivers using airborne digital imagery. Water Resources Research. 40: W07202.

Carling P, Beven K. 1989. The hydrology, sedimentology, and geomorphological implications of floods: An overview. In: Beven K, Carling P (eds.). Floods: Hydrological, sedimentological, and geomorphological implications, 1–9. Chichester, Wiley.

Carling P, Villanueva I, Herget J, Wright N, Borodavko P, Morvan H. 2000. Unsteady 1D and 2D hydraulic models with ice dam break for Quaternary megaflood, Altai Mountains, southern Siberia. Global Planetary Change 70: 24-34.

Carling P, Villanueva I, Harget J, Wright N, Borodavko P, Morvan H. 2010. Unsteady 1D and 2D hydraulic models with ice dam break for Quaternary megaflood, Altai Mountains, southern Siberia. Global and Planeraty Change 70: 24-34.

Casas A, Lane SN, Yu D, Benito G. 2010. A method for parameterising roughness and topographic sub-grid scale effects in hydraulic modelling from LiDAR data. Hydrology and Earth System Sciences 14: 1567-1579.

Chang HH. 1979. Geometry of Rivers in regime. Journal of the Hydraulics Division 105: 691-706.

Chandler J, Ashmore P, Paola C, Gooch M, Varkaris F. 2002. Monitoring river channel change using terrestrial oblique digital imagenary and automated digital protogrammetry. Annals of the Association of American Geographers 92: 631-644.

Chappel A, Heritage GL, Fuller IC, Large ARG, Milan DJ. 2003. Geostatistical analysis of ground-survey elevation data to eludicate spatial and temporal river channel change 28: 349-370.

Charlton ME, Large ARG, Fuller IC. 2003. Application of airborne LiDAR in river environments: the River Coquet, Northumberland, UK. Earth Surface Processes and Landforms 28: 299–306.

Chitale SV. 1973. Theories and relationship of river channel patterns. Journal of Hydrology 1973: 285-308.

Claude N, Rodrigues S, Bustillo V, Bréhét JG, Tassi P, Jugé P. 2014. Interactions between flow structure and morphodynamic of bars in a channel expansion/contraction, Loire River, France. Water Resources research 50: 2850-2873.

Coleman SE, Nikora VI. 2011. Fluvial dunes: initiation, characterization, flow structure. Earth Surface processes and landforms 36: 39-57.

Darby SE, Alabyan AM, Van de Wiel MJ. 2002. Numerical simulation of bank erosion and channel migration in meandering rivers. Water Resources Research 38: 2–21.

Dargahi B. 2004. Three-dimensional flow modelling and sediment transport in the river Klarälven. Earth Surface Processes and landforms 29: 821-852.

Davis WM. 1902. River terraces in New England. Bulletin of the Harvard University Museum of Comparative Zoology 38: 281-346.

Dean KG, Morrissey LA. 1988. Detection and identification of Arctic landforms - An assessment of remotely sensed data. Photogrammetric Engineering and Remote Sensing 54: 363-371.

Delft3D-FLOW. 2011. Simulation of multi-dimensional hydrodynamic flows and transport phenomena, including sediments. User Manual. Hydro-Morphodynamics, Version: 3.15, Revision: 18392, 7 September 2011.

Dietrich WE, Smith JD. 1983. Influence of the point bar on flow through curved channels. Water Resources Research 19: 1173–1192.

Dietrich WE, Smith JD. 1984. Bed load transport in a river meander. Water Resources Research 20: 1355-1380.
Dietrich WE, Smith JD, Dunne T. 1979. Flow and sediment transport in a sand bedded meander. Journal of Geology 87: 305–315.
Dinehart RL, Burau JR. 2005a. Repeated Surveys by Acoustic Doppler Current Profiler for Flow and Sediment Dynamics in a Tidal River. Journal of Hydrology 314: 1–21.
Dinehart RL, Burau JR. 2005b. Averaged indicators of secondary flow in repeated acoustic Doppler current profiler crossings of bends. Water Resources Research 41: W09405.
Dost R, Mannaerts C. 2008. Generation of lake bathymetry using sonar, satellite imagery and GIS, in ESRI 2008. Proceedings of the 2008 ESRI International User Conference: GIS, Geography in action. San Diego, US (4-8 Aug 2008).
Duan J, Wang SSY, Jia Y. 2001 The applications of the enhanced CCHE2D model to study the alluvial channel migration processes. Journal of Hydraulic Research 39: 469-480.
Duan JG, Julien PY. 2005. Numerical simulation of the inception of channel meandering. Earth Surface processes and Landforms 30: 1093-1110.
Dugdale SJ, Carbonneau PE, Campbell D. 2010. Aerial photosieving of exposed gravel bars for the rapid calibration of airborne grain size maps. Earth Surface Processes and Landforms 35: 627-639.
Dunbar, JA, Allen PM, Higley. 1999. Multifrequency acoustic profiling for water reservoir sedimentation studies. Journal of Sedimentary Research 69: 518-527.
Duncan CC, Klein AJ, Masek JG, Isacks BL 1998. Comparison of Late Pleistocene and Modern Glacier Extents in Central Nepal Based on Digital Elevation Data and Satellite Imagery. Quarternary Research 49: 241-254.
Edwards SJ, Cross PA, Barnes JB, Betaille D. 1999. A methodology for benchmarking real-time kinematic GPS. Survey Review 35: 163–174.
Einstein HA, 1942. Formulas for the transportation of bedload. Transaction of the American Society of Civil Engineers 107: 561-577.
Einstein HA. 1948. Determination of rates of bedload movement. In: Proceedings of the 1st Federal Inter-Agency Sedimentation Conference.
Einstein HA. 1950. The bedload function for sediment transportation in open channel flows. Technical Bulletin 1026. U.S. Department of Agriculture, Soil Conservation Service, Washington DC.
Emmett, W.W., 1980. A field calibration of the sediment-trapping characteristics of the Helley–Smith bedload sampler. USGS Professional Paper, 1139: 44 pp.
Engel FL, Rhoads BL. 2012. Interaction among mean flow, turbulence, bed morphology, bank failures and channel planform in an evolving compound meander loop. Geomorphology 163-164: 70-83.
Engelund F, Hansen E. 1967. A Monograph on Sediment Transport in Alluvial Streams. Teknisk Forlag, Copenhagen.
Engelund F. 1974. Flow and bend topography in channel bends. Journal of the Hydraulics Division 100: 1631-1648.
Engelund F, Fredsöe J. 1982. Sediment ripples and dunes. Annual Review of Fluid Mechanics 14: 13-37.
Ettema R. 2002. Review of alluvial-channel responses to river ice. Journal of Cold Regions Engineering 16: 191-217.
Farrel J, Givargis T. 2000. Differential GPS Reference Station Algorithm—Design and Analysis. IEEE Transactions on Control Systems Technology 8: 519-531.
Faro. 2014. http://www.faro.com/en-us/products/3d-surveying/faro-focus3d/features#main (4 Sept 2014).
Ferguson RI. 1987. Hydraulic and sedimentary controls of channel pattern. In: Richards KS (ed.). River Channels: environment and processes. Blackwell, Oxford.
Ferguson RI, Ashworth PJ. 1992. Spatial patterns of bedload transport and channel change in braided and near braided rivers. In: Billi P, Hey RD, Thorne CR, Tacconi P (eds.). Dynamics of Gravel-Bed Rivers. Wiley, Chichester.
Ferguson RI. 1994. Critical discharge for entrainment of poorly sorted gravel. Earth Surface Processes and Landforms 19: 719-186.
Ferguson RI, Parsons DR, Lane SN, Hardy RJ. 2003. Flow in meander bends with recirculation at the inner bank. Water Resources Research 11: 1322.
Finnish Meteorological Institute. 2014. http://en.ilmatieteenlaitos.fi/normal-period-1981-2010 (28 Sept 2014).
Flener C, Lotsari E, Alho P, Käyhkö J. 2012. Comparison of empirical and theoretical remote sensing based bathymetry models in river environments. River Research and Applications 28: 118-133.
Flener C, Vaaja M, Jaakkola A, Krooks A, Kaartinen H, Kukko A, Kasvi E, Hyyppä H, Hyyppä J, Alho P. 2013. Seamless mapping of river channels at high resolution using mobile LiDAR and UAV-photography. Remote Sensing 5: 6382-6407.

Flener C, Wang Y, Laamanen L, Kasvi E, Vesakoski JM, Alho P. Empirical modelling of spatial 3D flow characteristics using a remote-controlled ADCP system — monitoring a spring flood. Submitted to Water.

Fox RW, McDonald AT. 1978. Introduction to fluid mechanics, 2nd edition. John Wiley & Sons, New York.

Friedkin JF. 1945. A Laboratory Study of Meandering of Alluvial Rivers. United States Waterways Experiment Station, Vicksburg.

Friend PF, Sinha R. 1993. Braiding and meandering parameters. Geological Society, London, Special Publications. 75: 105-111

Frothingham KM, Rhoads BL. 2003. Three-dimensional flow structure and channel change in an asymmetrical compound meander, Embarras River, Illinois. Earth Surface Processes and Landforms 28: 625-644.

Fuller IC, Large ARG, Milan DJ. 2003. Quantifying channel development and sediment transfer following chute cutoff in a wandering gravel-bed river. Geomorphology 54: 307-323.

Gao Y, Li Z, McLellan JF. 1997. Carrier phase based regional area differential GPS for decimeter-level positioning and navigation. Proceedings of the 10th International Technical Meeting of the Satellite Division of The Institute of Navigation. Kansas City, US (16–19 Sept 1997).

Gargett AE. 1994. Observing Turbulence with a Modified Acoustic Doppler Current Profiler. Journal of Atmospheric and Oceanic Technology 11: 1592–1610.

Gautier E, Brunstein D, Vauchel P, Jouanneau JM, Roulet M, Garcia C, Guyot JL, Castro M. 2010. Channel and floodplain sediment dynamics in a reach of the tropical meandering Rio Beni (Bolivian Amazonia). Earth Surface Processes and Landforms 35: 1838-1853.

Gaweesh MTK, van Rijn LC. 1994. Bed-load sampling in sand-bed rivers. Journal of Hydraulic Engineering 120: 1364–1384.

Glysson GDG. 1993. U.S. geological survey bedload sampling policy. Hydraulic Engineering 1: 701–706.

Gilbert GK. 1914. The transportation of debris by running water. U.S. Geological Survey Professional Paper 86. Washington DC.

Gomez B. 1983. Temporal variations in bed load transport rates: the effect of progressive bed armouring. Earth Surface Processes and Landforms 8: 41-54.

Gomez B, Hubbel DV, Stevens HH. 1990. At-a-point bedload sampling in the presence of dunes. Water resources Research 26: 2717-2731.

Gomez B, Emmet WW, Hubbel DW. 1991. Comments on bedload sampling in small rivers. In: Proceedings of the 5th Federal Inter-Agency Sedimentation Conference.

Gomez B, Troutman BM. 1997. Evaluation process errors in bedload sam,pling using a dune model. Water Resources Research 33: 2387-2398.

Gordon L. 1996. Acoustic Doppler Current Profiler, Principles of Operation, A Practical Primer. RD Instruments. San Diego.

Gray JR, Gartner JW. 2009. Technological advances in suspended-sediment surrogate monitoring. Water Resources Research 45: W00D29.

Guerrero M, Lamnerti A. 2011. Flow field and morphology mapping using ADCP and multibeam techniques: survey in the Pro River. Journal of Hydraulic Engineering 137: 1576-1587.

Güneralp I, Marston RA. 2012. Process–form linkages in meander morphodynamics - Bridging theoretical modeling and real world complexity. Progress in Physical geography 36: 718-746.

Hardy RJ, Lane SN, Ferguson RI, Parsons DR. 2003. Assessing the credibility of a series of computational fluid dynamic simulations of open channel flow. Hydrological processes 17: 1539-1560.

Helley EJ, Smith W. 1971. Development and calibration of a pressure-difference bedload sampler. United States Department of the Interior, Geological Survey, Water Resources Division.

Héquette A, Hemdane Y, Anthony EJ 2008. Sediment transport under wave and current combined flows on a tide-dominated shoreface, northern coast of France. Marine Geology 249: 226-242.

Heritage GL, Fuller IC, Charlton ME, Brewer PA, Passmore DP. 1998. CDW photogrammetry of low relief fluvial features: accuracy and implications for reach-scale sediment budgeting. Earth Surface Processes and Landforms 23: 1219-1233.

Heritage GL, Hetherington D. 2007. Towards a protocol for laser scanning in fluvial geomorphology. Earth Surface Processes and Landforms 32: 66-74.

Heritage GL, Milan DJ. 2009. Terrestrial Laser Scanning of grain roughness in a gravel-bed river. Geomorphology 113: 4-11.

Hickin EJ. 1974. The development of meanders in natural river channels. American Journal of Science 274: 414-442.

Hicks DM, Gomez B. 2003. Sediment transport. In: Kondolf GM, Piégay H (eds.). Tools in Fluvial Geomorphology. John Wiley & Sons, Chichester.

Hjulström F. 1935. Studies of the morphological activity of rivers as illustrated by the River Fyris. Bulletin of the Geological Institute of the University of Uppsala 25: 221–527.

Hodge R, Brasington J, Richards K. 2009. In situ characterization of grain-scale fluvial morphology using Terrestrial Laser Scanning. Earth Surface Processes and Landforms 24: 954-968.
Hodgetts D. 2009. LiDAR in the Environmental Sciences: Geological Applications. In: Heritage GL, Large ARG (eds.). Laser Scanning for the Environmental Sciences. John Wiley & Sons, Chichester.
Hodskinson A, Ferguson RI. 1998. Numerical modelling of separated flow in river bends: Model testing and experimental investigation of geometric controls on the extent of flow separation at the concave bank. Hydrological Processes 12: 1323–1338.
Hohenthal J, Alho P, Hyyppä J, Hyyppä H. 2011. Laser scanning applications in fluvial studies. Progress in Physical Geography 35: 782-809.
Hooke RL. 1975 Distribution of sediment transport and shear stress in a meander bend. The Journal of geology 83: 543-565.
Hooke JM. 1984. Changes in river meanders: a review of techniques and results of analyses. Progress of Physical Geography 8: 473-508.
Hooke JM. 1995. Processes of channel planform change on meandering channels in the UK. In: Gurnell A, Petts GE (eds.). Changing river channels. Wiley, Chichester.
Hooke JM. 2007a. Spatial variability, mechanisms and propagation of change in an active meandering river. Geomorphology 84: 277–296.
Hooke JM. 2007b. Complexity, self-organisation and variation in behaviour in meandering rivers. Geomorphology 91: 236–258.
Hooke JM 2008. Temporal variations in fluvial processes on an active meandering river over a 20-year period. Geomorphology 100: 3-13.
Hooke JM, Yorke L. 2010. Rates, distributions and mechanisms of change in meander morphology over decadal timescales, River Dane, UK. Earth Surface Processes and Landforms 35: 1601-1614.
Hooke JM, Yorke L. 2011. Channel bar dynamics on multi-decadal timescales in an active meandering river. Earth Surface Processes and Landforms 26: 1910-1918.
Horritt MS, Bates PD. 2002. Evaluation of 1D and 2D numerical models for predicting river flood inundation. Journal of Hydrology 268: 87-99.
Horritt MS, Bates PD, Mattinson MJ. 2006. Effects of mesh resolution and topographic representation in 2D finite volume models of shallow water fluvial flow. Journal of Hydrology 329: 306-314.
Hubbel DW. 1964. Apparatus and techniques for measuring bed load . US Geological Survey Water-Supply Paper 1748.
Hubbell DW, Stevens HH, Skinner JV, Beverage JP. 1981. Recent refinements in calibrating bedload samplers. In: Water Forum 81. American Society of Civil Engineers, New York.
Hu GR, Khoo HS, Goh PC, Law CL. 2003. Development and assessment of GPS virtual reference stations for RTK positioning .Journal of Geodesy 77: 292–302.
Hyyppä J, Jaakkola A, Hyyppä H, Kaartinen, Kukko A, Holopainen M, Zhu L, Vastaranta M, Kaasalainen S, Krooks A, Litkey P, Lyytikäinen-Saarenmaa P, Matikainen L, Rönnholm P, Chen Y, Kivilahti A, Kosonen I. 2009. Map updating and change detection using vehicle- based laser scanning. 2009 Urban remote Sensing Joint Event.
Höfle B, Vetter M, Pfeifer N, Mandlburger G, Stötter J. 2009. Water surface mapping from airborne laser scanning using signal intensity and elevation data. Earth Surface Processes and Landforms 34: 1635-1649.
Ikeda S, Yamasaka M, Chiyoda M. 1987. Bed topography and 1 sorting in bends. Journal of Hydraulic Engineering 113: 190-206.
Inglis CC. 1937. The relationships between meander belts, distance between meanders on axis of stream, width, and discharge of rivers in flood plains and incised rivers. Annual Technical Report. Central Board of Irrigation, India.
Jackson, RG. 1975, Velocity-bedform-texture patterns of meander bends in the lower Wabash River of Illinois and Indiana. geological Society of America Bulletin 86: 1511-1522.
Jefferson M. 1902. Limiting width of meander belts. National geographic magazine 13: 373-384
Kaeser AJ, Litts TL, Tracy TW. 2013. Using Low-Cost Side-Scan Sonar For Benthic Mapping Throughout The Lower Flint River, Georgia, USA. River Research and Applications 29: 634–644.
Kaplan ED, Hegarty C. 2006. Understanding GPS: Principles and Applications. Artech House, Norwood.
Kennedy JF. 1969. The formation of sediment ripples, dunes and antidunes. Annual Reviews of Fluid Mechanics 1: 147-168.
Keim RF, Skaugset AE, Bateman DS. 1999. Digital terrain modeling of small stream channels with a total-station theodolite. Advances in Water Resources 23: 41-48.
Kleinhans MG. 2010. Sorting out river channel patterns. Progress in Physical Geography 34: 287–326.
Kleinhans MG, van den Berg JH. 2011. River channel and bar patterns explained and predicted by an empirical and a physics-based method. Earth Surface Processes and Landforms 26: 721–738.

Knighton AD. 1998. Fluvial Forms and Processes. A New Perspective. Arnold, London.
Khosronejad A, Rennie C, Salehi Neyshabouri S, Townsend R. 2007. 3D Numerical modeling of flow and sediment transport in laboratory channel bends. Journal of Hydraulic Engineering 133: 1123–1134.
Kukko A, Andrei C-O, Salminen V-M, Kaartinen H, Chen Y, Rönnholm P, Hyyppä H, Hyyppä J, Chen R, Haggrén H, Kosonen I, C˘apek K. 2007. Road environment mapping system of the Finnish Geodetic Institute – FGI Roamer. Proceedings of the ISPRS Workshop Laser Scanning 2007 and SilviLaser 2007. Espoo, Finland (12-14 Sept 2007).
Kukko, Jaakkola A, Lehtomäki M, Kaartinen H, Chen Y. 2009. Mobile mapping system and computing methods for modelling of road environment. Proceedings of the Urban remote Sensing Joint Event. Shanghai, China (20-22 May 2009).
Landau H, Vollath U, Chen X. 2002. Virtual reference station systems. Journal of Global Positioning Systems 1: 137-143.
Lane E. 1935. Stable channels in erodible materials. Transactions of the American Society of Civil Engineers 102: 123-142.
Lane SN, Richards KS, Chandler JH. 1992. Developments in photogrammetry; the geomorphological potential. Progress in Physical Geography 17: 306-328.
Lane SN, Chandler JH, Richards KS. 1994. Developments in monitoring and terrain modelling small-scale river-bed topography. Earth Surface Processes and Landforms 19: 349-368.
Lane SN, Richards KS, Chandler JH. 1996. Discharge and sediment supply controls on erosion and deposition in a dynamic alluvial channel. Geomorphology 15: 1-15.
Lane SN. 1998. Hydraulic modelling in hydrology and geomorphology: A review of high resolution approaches. Hydrological processes 12: 1131-1150.
Lane SN, Richards KS. 1998. High resolution, two-dimensional spatial modelling of flow processes in a multi-thread channel. Hydrological Processes 12: 1279-1298.
Lane SN, Bradbrook KF, Richards KS, Biron PA, Roy AG. 1999. The application of computational fluid dynamics to natural river channels: three-dimensional versus two-dimensional approaches. Geomorphology 29: 1–20.
Lane SN, Westaway RM, Hicks DM. 2003. Estimation of Erosion and Deposition volumes in a large, gravel-bed, braided river using synoptic remote sensing. Earth Surface Processes and Landforms 28: 249-271.
Lane SN, Tayefi V, Reid SC, Yu D, Hardy RJ. 2007. Interactions between sediment delivery, channel change, climate change and flood risk in a temperate upland environment. Earth Surface Processes and Landforms 32: 429-446.
Laustrup MS, Jacobson RB, Simpkins DG. 2007. Distribution of potential spawning habitat for sturgeon in the lower Missouri River. U.S. Geological Survey Open-File Report.
Large ARG, Heritage GL. 2009. Laser Scanning – evolution of the discipline. In: Heritage GL, Large ARG (eds.). Laser Scanning for the Environmental Scienes. Wiley, Chichester.
Leica Geosystems, 2014. http://hds.leica-geosystems.com/en/Leica-HDS6200_64228.htm (4 Sept 2014).
Lejot J, Delacourt C, Piegay H, Fournier T, Tremelo M-L, Allemand P. 2007. Very high spatial resolution imagery for channel bathymetry and topography from an unmanned mapping controlled platform. Earth Surface Processes and Landforms 32: 1705-1725.
Leopold LB, Wolman MG. 1957. River channel patterns: meandering, braiding and straight. geological Survey Professional Paper 282-B.
Leopold LB, Wolman MG. 1960. River meanders. Bulletin of the heological Society of America 71: 769-794.
Leopold L B, Wolman MG, Miller JP. 1964. Fluvial processes in geomorphology. WH Freeman, San Francisco.
Leopold LB; Langbein WB. 1966. River meanders. Scientific American 214: 60-70.
Lesser GR, Roelvink JA, kester TM, Stelling GS. 2004. Development and validation of a three-dimensional morphological model Coastal Engineering 51: 883-915.
Lewin J. Brewer PA. 2001. Predicting channel patterns. Geomorphology 40: 329-339.
Lien FS. Leschziner MA. 1994. Application of an RNG turbulence model to flow over a backwards-facing step. Computers and Fluids 23: 983-1004.
Lotsari E, Veijalainen N, Alho P, Käyhkö J. 2010. Impact of climate change on future discharges and flow characteristics of the tana river, sub-Arctic Northern Fennoscandia. Geografiska Annaler 92: 263-284.
Lotsari E, Wainwright D, Corner G, Alho P, Käyhkö J. 2014a. Surveyed and modelled one-year morphodynamics in the braided lower Tana River. Hydrological Processes 28: 2685-2716.
Lotsari E Vaaja M, Flener C, Kaartinen H, Kukko A, Kasvi E, Hyyppä H, Hyyppä J, Alho P. 2014b. Annual bank and point bar morphodynamics of a meandering river based on high-accuracy multi-temporal laser scanning and flow data. Water Resources Research 50: 5532-5559.
Low JW. 1952. Plane table mapping. Harper, New York.
Magiligan FJ.1992. Thresholds and the spatial variability of flood power during extreme floods. Geomorphology 5: 373-390.

Manning R. 1891. On the flow of water in open channels and pipes. Transactions of the Institution of Civil Engineers of Ireland. 20: 161–207.

Mansikkaniemi H, Mäki O-P. 1990. Paleochannels and recent changes in the Pulmankijoki valley, northern Lapland. Fennia 168: 137-152.

McGowen JH, Garner LE. 1970. Physiographic features and stratification types of coarse-grained point bars: modern and ancient examples. Sedimentology 14: 77-111.

Merckelbach, LM. 2006. A Model for High-Frequency Acoustic Doppler Current Profiler Backscatter from Suspended Sediment in Strong Currents. Continental Shelf Research 26: 1316–1335.

Meyer-Peter E, Müller R. 1948. Formula for Bed load Transport. Proceedings of the 2nd IAHR Meeting. Stockholm, Sweden (7–9 June 1984).

Micheletti N, Chandler JH, Lane SN. Investigating the geomorphological potential of freely available and accessible structure-from-motion photogrammetry using a smartphone. Earth Surface Processes and Landforms, *in press.*

Milan DJ, Heritage GL, Hetherington D. 2007. Application of a 3D laser scanner in the assessment of erosion and deposition volumes and channel change in a proglacial river. Earth Surface Processes and Landforms 32: 1657-1674.

Mockmore CA. 1944. Flow around bends in stable channels: Transaction of the American Society of Civil Engineers 109: 593H528.

Morales Y, Tsubouchi T. 2007. DGPS, RTK-GPS and StarFire DGPS performance under tree shading environments. Proceedings of the 2007 IEEE International Conference on Integration Technology. Shenzhen, China (20-24 March 2007).

Morche D, Schmidt KH, Sahling I, Herkommer M, Kutschera J. 2008. Volume changes of Alpine sediment stores in a state of post-event disequilibrium and the implications for downstream hydrology and bed load transport. Norwegian Journal of Geography 62: 89-101.

Mottershead DN, Duane WJ, Inkpen RJ, Wright JS. 2008. An investigation of the geometric controls on the morphological evolution of small-scale salt terrains, Cardona, Spain. Environmental geology 53:1091–1098.

Nelson JM, Logan BL, Kinzel PJ, Shimizu Y, Giri S, Shreve RL, Mclean SR. 2011. Bedform response to flow variability. Earth Surface Processes and Landforms 36: 1938-1947.

Nicholas AP, Smith GHS. 1999. Numerical simulation of three-dimensional flow hydraulics in a braided channel. Hydrological processes 13: 913-929.

Nicholas AP, 2000. Modelling bedload yield in braided gravel bed rivers. Geomorphology 36: 89-106.

Nicholas AP, Sandbach SD, Ashwoth PJ, Amsler ML, Best JL, Hardy RJ, Lane SN, Orfeo O, Parsons DR, Reesink AJH, Smith GHS, Szupiany RN. 2012. Modelling hydrodynamics in the Rio Paraná, Argentina: An evaluation and inter-comparison of reduced-complexity and physics based models applied to a large sand-bed river. Geomorphology 169-170: 192-211.

Nicholas AP. 2013. Modelling the continuum of river channel patterns. Earth Surface processes and Landforms 38: 1187-1196.

Notebaert B, Verstraeten G, Govers G, and Poesen J. 2009. Qualitative and quantitative applications of LiDAR imagery in fluvial geomorphology. Earth Surface Processes and Landforms 34: 217–231.

Nystrom E, Rehmann CR, Oberg KA. 2007. Evaluation of Mean Velocity and Turbulence Measurements with ADCPs. Journal of Hydraulic Engineering 133: 1310-1318.

Oberg K, Mueller DS. 2007. Validation of Streamflow Measurements Made with Acoustic Doppler Current Profilers. Journal of hydraulic Engineering 133: 1421-1432.

Oguchi T, Hayakawa Y, Wasklewicz T. 2011. Data sources. In: Smith MJ, Paron P, Griffiths J (eds.). Geomorphological Mapping: a handbook of Techniques and Applications. Elsevier, Amsterdam.

Ottevanger W, Blanckaert K, Uijttewaal WSJ. 2012. Processes governing the flow redistribution in sharp river bends. Geomorphology 163-164: 45-55.

Papanicolaou A, Elhakeem M, Krallis G, Prakash S, Edinger J. 2008. Sediment Transport Modeling Review—Current and Future Developments. Journal of Hydraulic Engineering 134: 1-14.

Parker G. 1976. On the cause and characteristic scales of meandering and braiding in rivers. Journal of Fluid Mechanics 76: 457- 480.

Parsons DR, Best JL, Orfeo O, Hardy RJ, Kostaschuk R, Lane SN. 2005. Morphology and flow fields of three-dimensional dunes, Rio Paraná, Argentina: Results from simultaneous multibeam echo sounding and acoustic Doppler current profiling. Journal of Geophysical Research: Earth Surface 110: F04S03.

Parsons DR, Best JL, Nale SN, Ofreo O, hardy R, Kostachuk R. 2007. Form roughness and the absence of secondary flow in a large confluence–diffluence, Rio Paraná, Argentina. Earth Surface Processes and Landforms 32: 155-162.

Petrie G, Toth CK. 2009. Introduction to laser ranging, profiling, and Scanning. In: Shan J, Toth CK (eds.). Topographic Laser ranging and scanning, principles and processing. Taylor & Francais Group, Boca Raton.

Petzold B, Reiss P, Stössel W. 1999. Laser scanning—surveying and mapping agencies are using a new technique for the derivation of digital terrain models. Journal of Photogrammetry and Remote Sensing 54: 95-104.

Pinto L, Fortunato AB, Freire P. 2006. Sensitivity analysis of noncohesive sediment transport formulae. Continental Shelf Research 26: 1826–1839.

Pizzuto J, O'Neal M, Stotts S. 2010. On the retreat of forested, cohesive riverbanks. Geomorphology 116: 341–352.

Playfair J. 1802. Illustrations of the Huttonian theory of the Earth. William Creech, Edinburgh.

Powell JW. 1875. Explorations of the Colorado River of the west and its tributaries: explored in 1869, 1870, 1871, and 1872 under the direction of the secretary of the Smithsonian Institution. Government Printer, Washington DC.

Prandtl L. 1945. Uber ein neues Formelsystem für die ausgebildete Turbulenz. Nachrichten von der Akademie der Wissenschaften in Gottingen. Mathematisch-Physikalische Klasse.

Pyrce R, Ashmore P. 2005. Bedload path length and point bar development in gravel bed river models. Sedimentology 52: 839-857.

Rathburn SL, Rubin ZK, Wohl EE. 2013. Evaluating channel response to an extreme sedimentation event in the context of historical range of variability: Upper Colorado River, USA. Earth Surface Processes and Landforms 38: 391-406.

Ray RG. 1960. Aerial photographs in geologic interpretation and mapping. Geological survey professional paper 737.

Rehmel M. 2007. Application of Acoustic Doppler Velocimeters for streamflow measurements. Journal of Hydraulic Engineering 133: 1433-1438.

Reid I, Layman JR, Frostick LE. 1980. The continuous measurement of bedload discharge. Journal of Hydraulic Research 18: 243–249.

Reinfelds I, Cohen T, Batten P, Brierley G. 2004. Assessment of downstream trends in channel gradient, total and specific stream power: a GIS approach. Geomorphology 60: 403–416.

Rennie CD, Millar RG, Church MA. 2002. Measurement of bed load velocity using an Acoustic Doppler Current Profiler. Journal of Hydraulic Engineering 128: 473-483.

Rennie CD, Church M. 2010. Mapping spatial distributions and uncertainty of water and sediment flux in a large gravel bed river reach using an acoustic Doppler current profiler. Journal of Geophysical Research: Earth Surface 115: F03035

Retscher G. 2002. Accuracy performance of virtual reference station (VRS) networks, Journal of Global Positioning Systems 1: 40-47.

Rhoades EL, O'Neal MA, Pizzuto JE. 2009. Quantifying bank erosion on the South River from 1937 to 2005, and its importance in assessing Hg contamination. Applied Geography 29: 125–134.

Rinaldi M, Darby S E. 2008. Modelling river-bank-erosion processes and mass failure mechanisms: progress towards fully coupled simulations. In: Habersack H, Piégay M, Rinaldi M (eds.). Gravel-bed Rivers VI: From Process Understanding to River Restoration. Elsevier, Oxford.

van Rijn LC. 1984a. Sediment transport, part I: bed load transport. Journal of Hydraulic Engineering 110: 1431–1456.

van Rijn LC. 1984b. Sediment transport, part II: suspended load transport. Journal of Hydraulic Engineering 110: 1613–1640.

van Rijn LC. 1993. Principles of sediment transport in rivers, estuaries and coastal seas. Aqua Publications, Amsterdam.

Ritchie W, Wood M, Wright R, Tait D. 1988. Surveying and Mapping for field scientists. Longman Scientific & Technical, New York.

Rizos C. 2002. Network RTK research and implementation – A geodetic perspective, Journal of Global Positioning Systems 1: 144-150

Robert A. 2003. River processes: An introduction to Fluvial Dynamics. Arnold, London.

Rodi W. 1980. Turbulence Models and their Application in Hydraulics. IAHR, Delft. 104 p

Rodriguez JF, Bombardelli FA, Garcia MH, Frothingam KM, Rhoads BL, Abad JD. 2004. High-resolution numerical simulation of flow through a highly sinuous river reach. Water Resources Management 18: 177–199.

Rouse, H., 1937. Modern conceptions of the mechanics of fluid turbulence. Transactions of the American Society of Civil Engineers 102: 463–554.

Rozovskii IL. 1957. Flow of water in bends of open channels. Academy of Sciences of the Ukrainian SSR, Kiev.

Rüther N, Jacobsen J, Reidar N, Olsen B, Vatne G. 2010. Prediction of the three-dimensional flow field and bed shear stresses in a regulated river in mid-Norway Hydrology Research 41:145–152.

Rüther N, Olssen NRB. 2007. Modelling free-forming meander evolution in a laboratory channel using three-dimensional computational fluid dynamics. Geomorphology 89: 308-319.

Ryan SE, Porth L, Troendle C. 2005. Coarse sediment transport in mountain streams in Colorado and Wyoming, USA. Earth Surface Processes and Landforms 30: 269–288.

Schumm SA. 1963. Sinuosity of Alluvial Rivers on the Great Plains. Geological Society of America Bulletin. 74: 1089-1100.

Schumm SA, Khan HR. 1972. Experimental Study of Channel Patterns. Geological Society of America Bulletin. 83: 1755-1770.

Schumm SA. 1985. Patterns of Alluvial Rivers. Annual Review of Earth and Planetary Sciences 13: 5-27.

Schuurman F, Marra AW, Kleinhans MG. 2013. Physics-based modeling of large braided sand-bed rivers: Bar pattern formation, dynamics, and sensitivity. Journal of geophysical research: Earth Surface 118: 2509-2527.

Seminara G. 2010. Fluvial Sedimentary patterns. Annual Review of Fluid Mechanics 42: 43-66.

Shields A. 1936. Anwendung der Aenlichkeitsmechanik und der Turbulenzforschung auf die Geschiebebewegung. Mitteilungen der Preussischen Versuchsanstalt fur Wasserbau und Schiffbau, Berlin, Germany. California Institute of Technology, Pasadena.

Shimizu Y, Yamaguchi H, Itakura T. 1990. Three-dimensional computation of flow and bed deformation. Journal of Hydraulic Engineering 116: 235-253.

Simpson JH, Mitchelson-Jacob EG, Hill AE. 1990. Flow structure in a channel from an acoustic Doppler current profiler. Continental Shelf Research 10: 589-603.

Sithole G, Vosselman, G. 2004. Experimental comparison of filter algorithms for bare-earth extraction from airborne laser scanning point clouds. ISPRS Journal of Photogrammetry and Remote Sensing 59: 85–101.

Smith HTU. 1941. Aerial photographs in geomorphic studies. Journal of Geomorphology 4: 171-205.

Sontek/YSI. 2010. RiverSurveyor S5/M9 System Manual, Firmware Version 1.0. Sontek/YSI Incorporated, San Diego.

Statham I. 1990. Slope processes. In: (eds.). Goudie AS. Geomorphological techniques.

Stott T. 2013. Review of research in fluvial geomorphology 2010-2011. Progress in Physical Geography 37: 248-258.

Termini D, Piraino M. 2011. Experimental analysis of cross-sectional flow motion in a large amplitude meandering bend. Earth Surface Processes and Landforms 36: 244-256.

Thoma DP, Hupta SC, Bauer ME, Kirchoff CE. 2005. Airborne laser scanning for riverbank erosion assessment. Remote Sensing of Environment 95: 493-501.

Thompson A. 1986. Secondary flows and the pool-riffle unit: a case study of the processes of meander development. Earth Surface Processes and Landforms 6: 631–641.

Thorne CR, Zevenbergen LW, Pitlick JC, Rais S, Bradley JB, Julien PY. 1985. Direct measurements of secondary currents in a meandering sand-bed river. Nature 315: 746-747.

Tieje AJ. 1929. The study of geology by aeroplane. Science 69: 301-302.

Vaaja M, Hyyppä J, Kukko A, Kaartinen H, Hyyppä H, Alho P. 2011. Mapping topography changes and elevation accuracies using a mobile laser scanner. Remote Sensing 3: 587-600.

Veijalainen *et al* 2010

Vollath U, Buecherl A, Landau H, Pagels C, Wagner B. 2000. Multi-base RTK positioning using virtual reference stations, Proceedings of the 13th International Technical Meeting of the Satellite Division of The Institute of Navigation. Salt Lake City, US (19-22 Sept 2000).

Vosselman G, Maas H-G. 2010. Airborne and Terrestrial Laser Scanning. Whittles Publishing: Dunbeath.

Voulgaris G, Trowbridge JH. 1998. Evaluation of the Acoustic Doppler Velocimeter (ADV) for turbulence measurements. Journal of the Atmospheric and Oceanic Technology 15: 272-289.

Warburton J, Davies TRH, Mandl MG. 1993. A meso-scale field investigation of channel change and floodplain characteristics in an upland braided gravel-bed river, New Zealand. In Braided Rivers, Best JL, Bristow CS (eds.) Geological Society Special Publication 75:73-87.

Westaway RM, Lane SN, Hicks DM. 2003. Remote survey of large-scale braided rivers using digital photogrammetry and image analysis. International Journal of Remote Sensing 24: 795–816.

Wheaton JM, Brasington J, Darby SE, Sear DA. 2010. Accounting for uncertainty in DEMs from repeat topographic surveys: improved sediment budgets. Earth Surface Processes and Landforms 35: 136–156.

Williams RD. Brasington J. Hicks M. Measures R. Rennie C. 2013. Vericat, D. Hydraulic validation of two dimensional simulations of braided river flow with spatially continuous aDcp data. Water Resources Research 49: 5183–5205.

Williams RD, Brasington J, Vericat D, Hicks DM. 2014. Hyperscale terrain modelling of braided rivers: fusing mobile terrestrial laser scanning and optical bathymetric mapping. Earth Surface Processes and Landforms 39: 167-183.

Wilson CAME, Boxall JB, Guymer I, Olsen NRB. 2003. Validation of a three-dimensional numerical code in the simulation of pseudo-natural meandering flows. Journal of Hydraulic Engineering 129: 158-168.

Winterbottom SJ, Gilvear DJ. 1997. Quantification of channel bed morphology in gravel-bed rivers using airborne multispectral imagery and aerial photography. River Research and Applications 13: 489-499.

Wohl E. 2014. Time and the rivers flowing: Fluvial geomorphology since 1960. Geomorphology 216: 263-282.

Wolman MG, Leopold LB., 1957. River flood plains: some observations on their formation. U.S. Geological Survey Professional Paper 282-C, Washington, DC.

Wu B, Maren DS, Li L. 2008. Predictability of sediment transport in the Yellow River using selected transport formulas. International Journal of sediment Research 23: 283-298.

Yakhot V, Orszag SA, Thangam S, Gatshi TB, Speziale CG. 1992. Development of a turbulence model for shear flow by a double expansion technique. Physics of Fluids A4: 1510-1520.

Yakhot V, Orszag SA. 1986. Renormalization group analysis of turbulence. I. Basic theory. Journal of Scientific Computing 1: 3-51.

Yorke TH, Oberg KA. 2002. Measuring river velocity and discharge with acoustic Doppler profilers. Flow Measurement and Instrumentation 13: 191-195.